Article

Bright Green Biofluorescence in Sharks Derives from Bromo-Kynurenine Metabolism

Swell Shark (*Cephaloscyllium ventriosum*)

Bright-Field Image

Fluorescence Image

Denticle Structure of Chain Catshark (*Scyliorhinus retifer*)

Hyun Bong Park, Yick Chong Lam, Jean P. Gaffney, ..., Vincent Pieribone, David F. Gruber, Jason M. Crawford

david.gruber@baruch.cuny. edu (D.F.G.)
jason.crawford@yale.edu (J.M.C.)

HIGHLIGHTS

We describe a new form of biofluorescence from the skin of catsharks

Bromo-tryptophan-kynurenines are biofluorescent and show antimicrobial activities

Specific dermal denticles in the chain catshark act as optical light-guides

This study opens questions related to biological function of shark fluorescence

iScience

CellPress

Article

Bright Green Biofluorescence in Sharks Derives from Bromo-Kynurenine Metabolism

Hyun Bong Park,[1,2] Yick Chong Lam,[1,2] Jean P. Gaffney,[3,4] James C. Weaver,[5] Sara Rose Krivoshik,[3,4] Randy Hamchand,[1,2] Vincent Pieribone,[6] David F. Gruber,[3,4,*] and Jason M. Crawford[1,2,7,8,*]

SUMMARY

Although in recent years there has been an increased awareness of the widespread nature of biofluorescence in the marine environment, the diversity of the molecules responsible for this luminescent phenotype has been mostly limited to green fluorescent proteins (GFPs), GFP-like proteins, and fluorescent fatty acid-binding proteins (FABPs). In the present study, we describe a previously undescribed group of brominated tryptophan-kynurenine small molecule metabolites responsible for the green biofluorescence in two species of sharks and provide their structural, antimicrobial, and spectral characterization. Multi-scale fluorescence microscopy studies guided the discovery of metabolites that were differentially produced in fluorescent versus non-fluorescent skin, as well as the species-specific structural details of their unusual light-guiding denticles. Overall, this study provides the detailed description of a family of small molecules responsible for marine biofluorescence and opens new questions related to their roles in central nervous system signaling, resilience to microbial infections, and photoprotection.

INTRODUCTION

Biofluorescence is a widespread phenomenon in the marine environment, which results from the absorbance of the dominant ambient blue ocean light and its re-emittance at longer, lower-energy wavelengths, visually resulting in green, orange, and red fluorescence. Following the seminal 1962 discovery of green fluorescent protein (GFP) from *Aequorea victoria*, a hydrozoan medusa (Shimomura et al., 1962), fluorescent proteins (FPs) have since been described from cnidarians (Gruber et al., 2008; Matz et al., 1999), crustaceans (Meyers et al., 2004), and cephalochordates (Deheyn et al., 2007). The discovery of GFP has led to numerous breakthroughs in biomedical science (Gruber and Pieribone, 2006) following the exhibition of its heterologous expression (Chalfie et al., 1994) and mutations that led to brighter and spectrally modulatable variants (Tsien, 1998). GFP-like fluorescent proteins have since been identified in a wide range of other cnidarians, including corals, anemones, hydroids, pennatulids, and corallimorpharians and are now recognized as a ubiquitous metazoan protein superfamily (Shagin et al., 2004).

Within fishes, biofluorescence was only recently reported to be a phylogenetically widespread and phenotypically variable phenomenon that encompasses at least 16 orders, 50 families, 105 genera, and over 180 species (Sparks et al., 2014). Yet among this multitude of biofluorescent fish species, the chemistry had only been elucidated in the eels, *Anguilla japonica* (Hayashi and Toda, 2009; Kumagai et al., 2013), *Kaupichthys hyoproroides*, and *Kaupichthys* n. sp (Gruber et al., 2015), all of which are bilirubin-inducible fluorescent proteins. Here, we focus on the chemical mechanism of biofluorescence in two species of elasmobranchs, both in the family Scyliorhinidae, with *Cephaloscyllium ventriosum* (the swell shark) being endemic to the eastern Pacific (Compagno, 1984) and *Scyliorhinus retifer* (the chain catshark) from the western Atlantic (Castro, 2011).

Regional biofluorescence of the skin of these sharks has previously been shown to exhibit a higher intensity of the green-dominated fluorescence in the lighter, beige-colored areas, compared with the darker reticulated lines for the chain catshark or the dark spots for the swell shark (Figure 1) (Gruber et al., 2016). Through comparative metabolic profiling studies between these two distinctly pigmented tissue types, we report the discovery of a suite of small molecule metabolites stimulated in the light skin tissue, relative to the dark skin tissue from these two shark species. Specifically, high-resolution mass spectrometry (MS), UV-visible spectroscopy, multidimensional nuclear magnetic resonance (NMR), and fluorescence spectroscopy were used to unambiguously identify and characterize a family of brominated tryptophan-kynurenine metabolic products that are responsible for the biofluorescence phenotype in these two species of shark. Although GFP, GFP-like proteins, and bilirubin-binding fluorescent proteins have been reported from a variety of invertebrate (Gruber et al., 2008; Matz et al., 1999) and vertebrate (Gruber et al., 2015; Hayashi and

[1]Department of Chemistry, Yale University, New Haven, CT 06520, USA

[2]Chemical Biology Institute, Yale University, West Haven, CT 06516, USA

[3]Department of Natural Sciences, City University of New York Baruch College, New York, NY 10010, USA

[4]The Graduate Center Program in Biology, City University of New York Baruch College, New York, NY 10016, USA

[5]Wyss Institute for Biologically Inspired Engineering, Harvard University, Cambridge, MA 02138, USA

[6]The John B. Pierce Laboratory, Department of Cellular and Molecular Physiology, Yale School of Medicine, New Haven, CT 06519, USA

[7]Department of Microbial Pathogenesis, Yale School of Medicine, New Haven, CT 06536, USA

[8]Lead Contact

*Correspondence: david.gruber@baruch.cuny.edu (D.F.G.), jason.crawford@yale.edu (J.M.C.)

https://doi.org/10.1016/j.isci.2019.07.019

iScience

CellPress
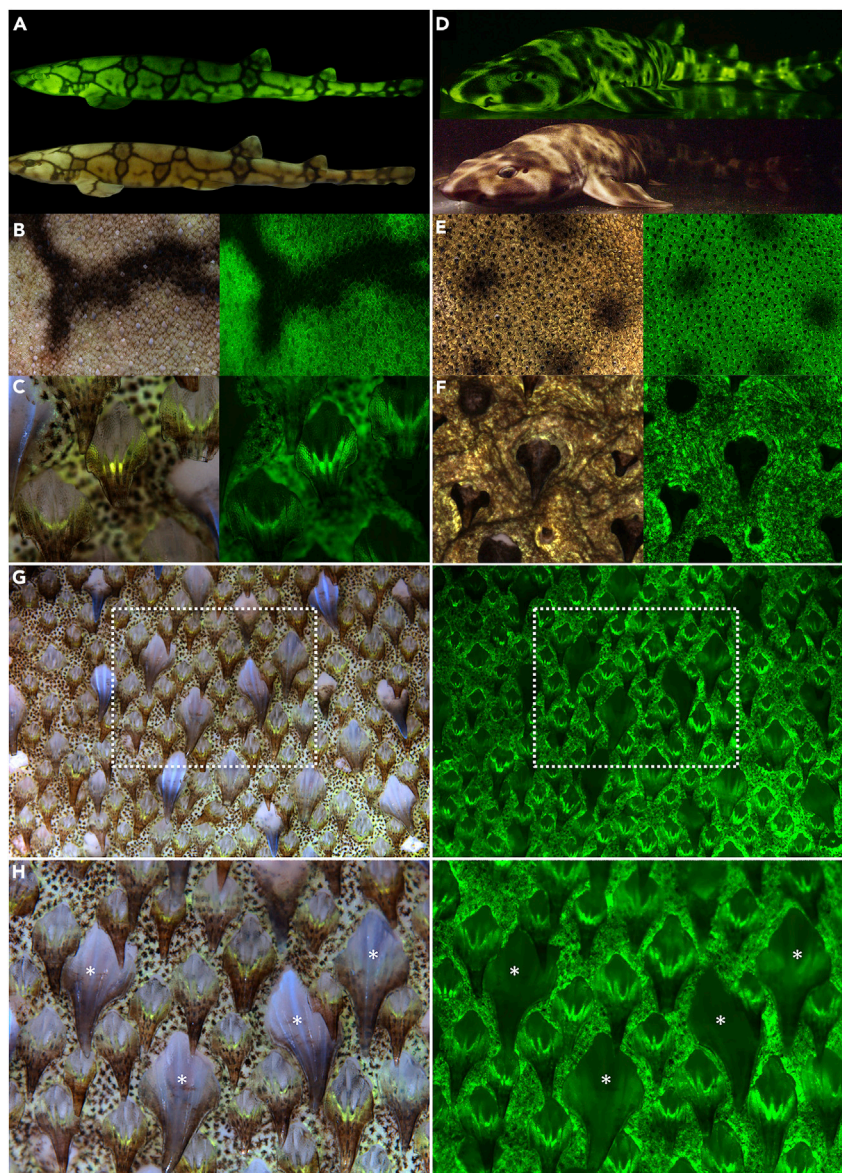
Figure 1. Fluorescent Shark Imaging

(A–H) Bright-field and fluorescence imaging of *Scyliorhinus retifer* (A–C) and *Cephaloscyllium ventriosum* (D–F). In contrast to the dark denticles from *C. ventriosum*, those from *S. retifer* act as efficient optical waveguides, effectively channeling the fluorescence signal along their length. *S. retifer* has a second type of larger, non-light-guiding denticles (G and H), and bright-field (left) and fluorescence (right) imaging reveals that the larger non-light-guiding denticles can easily be distinguished through bright-field imaging (due to their ability to weakly scatter blue light from their longitudinal surface ridges). A patch of both denticle types is shown in (G), whereas the larger non-light-guiding denticles are highlighted with asterisks in (H). Image widths: B, 20 mm; C, 1.2 mm; E, 20 mm; F, 1.5 mm; G, 7 mm; H, 3.3 mm.

Toda, 2009; Kumagai et al., 2013) taxa, these brominated tryptophan-kynurenine metabolites from elasmo-branchs represent a previously undescribed family of biofluorescent small molecule metabolites.

RESULTS

Skin Tissue Structure in Microscopy

C. ventriosum has small intensely green fluorescent spots over much of the body (Video S1), which appear light beige under white light. *S. retifer*, in contrast, exhibits an alternating light and dark reticulated pigmentation

iScience

CellPress

pattern, but it lacks the brightly fluorescent spots characteristic of *C. ventriosum* (Figure 1). Excised skin pieces from *C. ventriosum* and *S. retifer* were examined in their native state using a dual-camera Zeiss Axio zoom v16 fluorescence microscope. For sequential data collection from identical areas, the bright-field images were acquired with a Zeiss 506 color digital camera and the green fluorescence images were acquired with a Hamamatsu Flash 4.0 black and white digital camera. We note a surprising finding that the dermal denticles of *C. ventriosum* are not fluorescent, whereas those of *S. retifer* act as efficient optical waveguides, channeling the fluorescent signal along their length (Figure 1). Further analysis of *S. retifer* denticle structural diversity revealed that in addition to the smaller light-guiding denticles, a second type of larger, non-light-guiding denticles are also present (Figures 1G and 1H). This shows that the green fluorescence is not only targeted to varying regions of the shark but also that the targeting is fine-tuned to specific denticle types within a shark species. It has been previously demonstrated that these shark species possess the visual apparatus to detect biofluorescence (484 and 488-nm monochromat visual pigments in *C. ventriosum* and *S. retifer*, respectively) and that there are pronounced sexually dimorphic fluorescent patterns (Gruber et al., 2016). The green biofluorescence thus creates greater visual contrast for these sharks at depth, due to the primarily blue mesophotic marine environment (Gruber et al., 2016). It has also been shown that there are species-specific emission patterns in other fluorescent fish species, leading to the suggestion that biofluorescence functions in intraspecific communication and assists camouflage (Sparks et al., 2014). These observations of biofluorescent targeting to specific denticle types further advances our understanding of the complexity of this unique biofluorescence in the shark skin and the possible optical functions it may play. It is also noteworthy, that the deep-sea lanternshark (*Etmopterus spinax*) has also been shown to utilize its mineralized spines for the transmission of bioluminescent signals (Claes et al., 2013).

Brominated Metabolites in Swell Shark Skin Tissue

To establish a molecular basis for shark skin biofluorescence, we first analyzed small molecule extracts of dark and light skin tissue samples from the swell shark (*C. ventriosum*). Skin tissues were dissected using a fluorescence microscope (Zeiss-Axio Zoom V16 stereo fluorescent microscope) affixed with a Nikon D4 camera. The organic crude extracts of skin tissue samples were analyzed using an ultrahigh-performance liquid chromatography (UPLC) system equipped with a photodiode array detector and a high-resolution electrospray ionization-quadrupole time-of-flight-mass spectrometer (HR-ESI-QTOF-MS) (Figures 2A and S1). We first analyzed two major metabolites **4** and **5** eluting at retention times 19.2 and 11.2 min, respectively, which were similarly present in both the dark and light tissue samples (Figures 2A and S2). Their high-resolution mass spectra in positive mode showed an isotope distribution pattern attributable to the presence of bromine atoms at m/z 528.9875, 530.9859, and 532.9843 (relative intensity 1:2:1) for **4** and at m/z 283.0109 and 285.0090 (relative intensity 1:1) for **5**, indicating the molecular formulas of **4** and **5** to be $C_{22}H_{18}Br_2N_4O_2$ and $C_{11}H_{11}BrN_2O_2$, respectively (Table S1 and Figure S1). In addition, UV-visible spectra of these peaks shared a characteristic indole chromophore, suggesting the presence of a brominated tryptophan moiety known to be fluorescent (Figures S7A and S8A) (Schnepel et al., 2016). The chemical structures of these metabolites isolated from swell shark skin were fully elucidated using ^1H and gradient-enhanced 2D NMR (correlation spectroscopy, heteronuclear single-quantum coherence with adiabatic pulses, and heteronuclear multiple-bond correlation with adiabatic pulses) and Marfey's analysis (Figures S7, S8, S15, and S16, and Table S3). The NMR interpretation of these metabolites revealed resonances and correlations attributable to a 6-bromo tryptophan-derived diketopiperazine (**4**) and its monomer substrate (**5**), respectively (Figure 2B). Marfey's analysis on **4** and **5** allowed us to establish their structures as (9*S*, 9'*R*)-6-bromo-tryptophan-derived diketopiperazine and 9*S*-bromo-tryptophan, respectively (Figures S7C and S8C).

We then focused on small molecules differentially produced in light and dark skin tissue samples. We detected five major metabolites (**1–3**, **7**, and **8**) that were significantly stimulated in the light samples relative to the dark samples (Figure 2A). The UV-visible spectrum of metabolite **1** was similar to that of kynurenine (Figure S4A), a major product of tryptophan catabolism in mammals (Cervenka et al., 2017; Kolodziej et al., 2011). However, the HR-ESI-QTOF-MS data of **1** (m/z 287.0032 and 289.0013 [relative intensity 1:1]) similarly supported the presence of a bromine atom in its chemical formula ($C_{10}H_{11}BrN_2O_3$) (Figure S1 and Table S1), suggesting that the structure of **1** could be a bromo-kynurenine. The chemical formulas of **2**, **3**, **7**, and **8** were deduced as $C_{11}H_{11}BrN_2O_4$, $C_{10}H_9BrNO_3$, $C_7H_6BrNO_2$, and $C_{10}H_9BrNO_3$, respectively, and UV-visible spectroscopic data suggested that they were additional brominated metabolites processed through the kynurenine pathway: *N*-formyl-bromo-kynurenine (**2**), bromo-CKA (carboxyketoalkene derivative of kynurenine) (**3**), bromo-anthranilic acid (**7**), and bromo-kynurenine yellow (**8**) Figures 2B, S5A, S6A, S10A, and S11A and Table S1).

iScience

CellPress
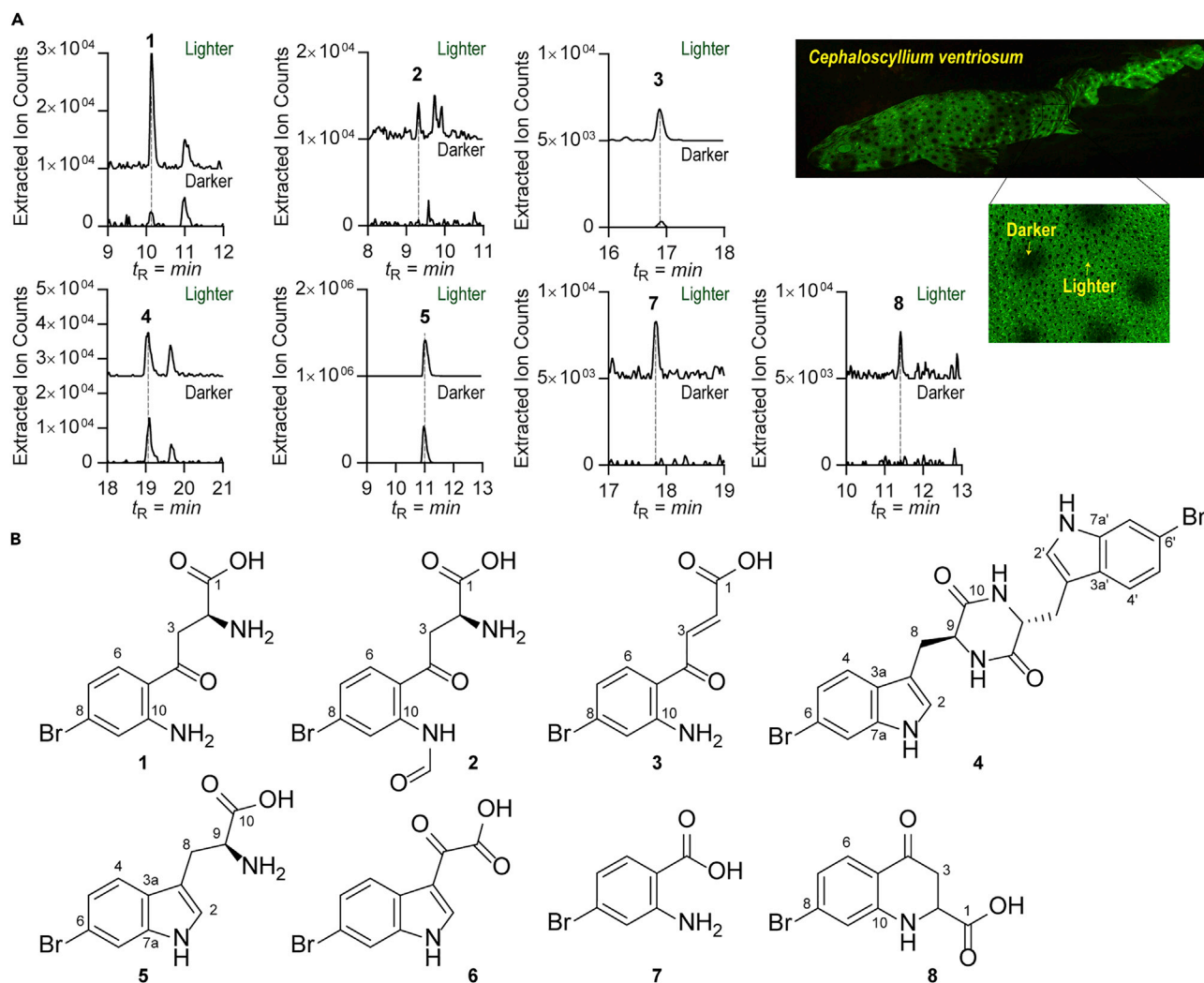
Figure 2. Comparative Metabolic Profiles of Skin Extracts from *Cephaloscyllium ventriosum*

(A) Differential extracted ion counts chromatograms corresponding to eight representative metabolites from light and dark areas of skin.

(B) Chemical structures of metabolites **1–8**. **1–4** and **8** represent previously unknown metabolites.

The structural characterization of metabolites **1–3** was achieved through chemical synthesis (Figures S3A and S12–S14, and Table S2). Briefly, a substrate, 6-bromo-L-tryptophan (**5**), was prepared and *meta*-chloroperoxybenzoic acid (0.32 g, 1.854 mmol, 10.5 equiv.) was added. The chemical reaction was stirred at room temperature under air atmosphere for 20 h to yield the 8-bromo-*N*-formyl-L-kynurenine (**2**). Deformylation with 50% trifluoroacetic acid (TFA) led to the product 8-bromo-L-kynurenine (**1**), which was deaminated under 70°C to give the 8-bromo-CKA (**3**) (Figure S3A). Co-injection and Marfey's analysis with synthetic and natural materials unambiguously confirmed the absolute chemical structures of these metabolites (Figures S4–S6). The structure of **7** was determined as 4-bromo-anthranilic acid by comparison of UV spectra and liquid chromatography (LC)-MS co-injection with a commercial standard (Figure S10). Last, we chemically synthesized compound **8** employing a synthetic scheme analogous to a previous report (Higgins et al., 2009) (Figures S3B, S17, and S18 and Table S4), and co-injection studies with the synthetic standard and the natural skin material confirmed the proposed structure of **8** (Figure S11).

Brominated Metabolites in Chain Catshark Skin Tissue

We next examined whether these metabolites existed in the biofluorescent chain catshark, *S. retifer*. Comparative metabolic analysis revealed that the same brominated metabolites are also present in chain

iScience

CellPress
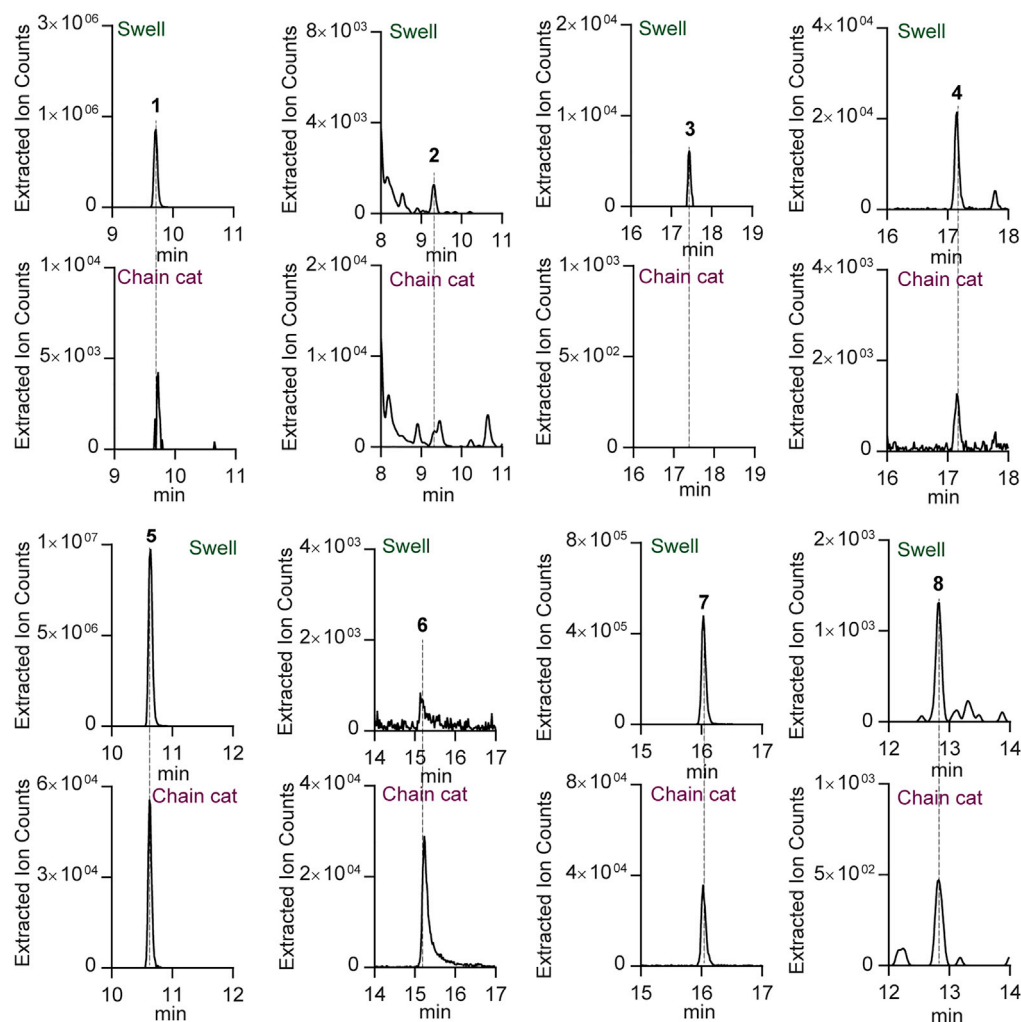
Figure 3. Comparative Metabolic Analysis of Skin Extracts from *Cephaloscyllium ventriosum* (Swell Shark) and *Scyliorhinus rotifer* (Chain Catshark)

catsharks (Figure 3), although metabolite **3** was below the detection limit under the conditions of our experiments. In addition, we identified major metabolite **6**, a brominated variant of indole-3-glyoxylic acid in *S. retifer* and confirmed its structure by co-injection experiments with an authentic standard (Figure S9). These studies identified a total of eight small molecule metabolites from biofluorescent shark skins.

Kynurenine Metabolism

The structures of the brominated metabolites in biofluorescent shark skins suggest that the brominated tryptophan found in both dark and light skin tissues is promiscuously processed through the tryptophan-kynurenine pathway (Figure 4). In humans, kynurenine metabolism is known to regulate important biological processes, including host-microbiome signaling and immune response, and is also linked to the pathogenesis of a variety of diseases such as diabetes, inflammation, neurodegenerative disorders, and cancer (Cervenka et al., 2017; Mazarei and Leavitt, 2015; Van der Leek et al., 2017). As enzymes involved in kynurenine metabolism can also be found in diverse bacteria (Bortolotti et al., 2016; Forouhar et al., 2007; Kurnasov et al., 2003), we tested if the common gut inhabitant *E. coli* is capable of metabolizing 6-bromo-L-tryptophan to 8-bromo-L-kynurenine. Indeed, *E. coli* Nissle 1917 biotransformed 6-bromo-L-tryptophan to 8-bromo-L-kynurenine in the ratio of 64:1, as determined by LC-MS (Figure S19), further supporting flexibility in functionalized tryptophan catabolism.

iScience

CellPress
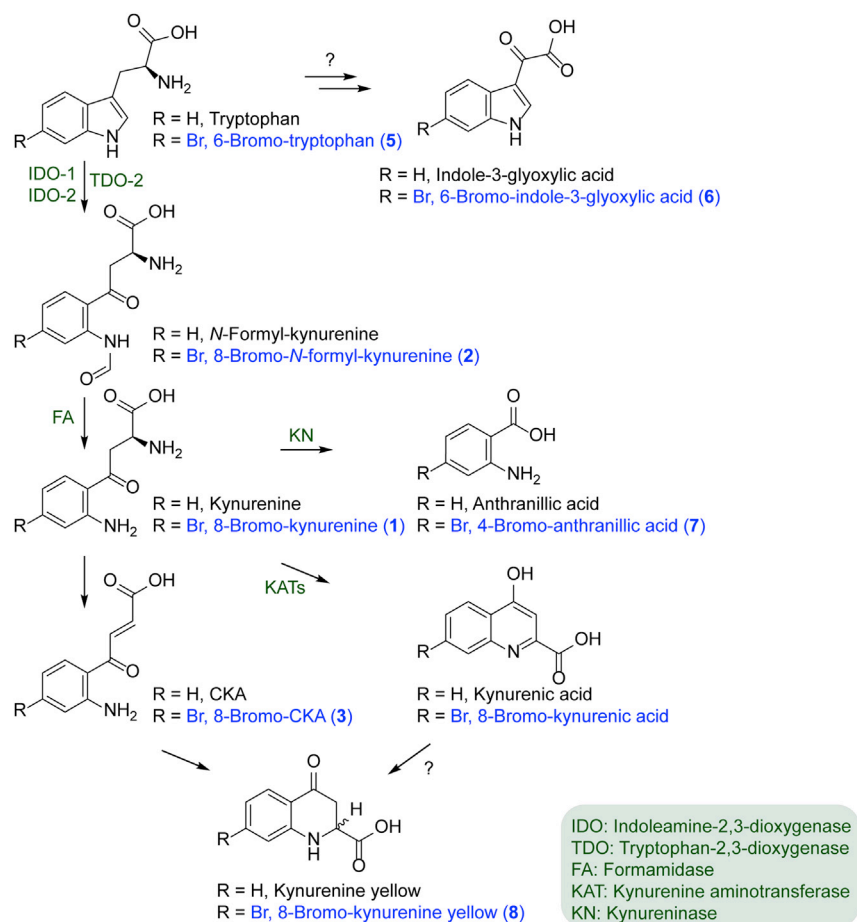
Figure 4. Overview of the Kynurenine and Bromo-kynurenine Pathway

Bromo-tryptophan appears to be promiscuously processed through the kynurenine pathway to generate the biofluorescent shark metabolites.

Absorbance and Fluorescence Emission of Metabolites

The absorbance and fluorescence excitation and emission spectra were taken for the characterized compounds. First, absorbance and fluorescence spectra of all compounds were measured at 5 mM concentrations in methanol. Based on the absorbance of the compounds, initial excitations were run using the absorbance values.

Compounds **1** and **7** were found to have similar excitation and emission spectra as L-kynurenine and were found to have two excitation peaks (Figure 5). However, of the two excitation peaks, one was found to cause a much stronger fluorescence emission. Peak absorbance of **1** and **7** was found to be 375 nm, whereas the excitation spectra were found to be maximal at 407 and 374 nm, respectively. Emission spectra for **1** and **7** were found to be in the blue wavelength range at 447 nm (**1**) and 439 nm (**7**) (Figures 5A and 5G).

Compounds **2–5** and **6** were found to have similar excitation and emission spectra as L-tryptophan (Figure 5). Unlike **1** and **7**, these compounds were only excited by one peak. Compounds **2**, **4,** and **5** were found to emit in the blue wavelength with emissions close to 450 nm (453, 448, and 454 nm, respectively) and were excited at 370 nm. Compound **3** was found to exhibit significantly red-shifted fluorescence than the other compounds, which exhibited a blue wavelength emission peak of 477 nm with broad green spectrum tailing. Similarly, compound **6** was found to have a blue wavelength emission, although it trailed into the green spectra with a peak emission of 484 nm. Non-brominated kynurenine yellow is known to exhibit bright green fluorescence with an emission maxima of ~520 nm (Mizdrak et al., 2007; Zelentsova et al., 2013), whereas our experimental fluorescence spectrum of bromo-kynurenine yellow (**8**) obtained in

iScience

CellPress
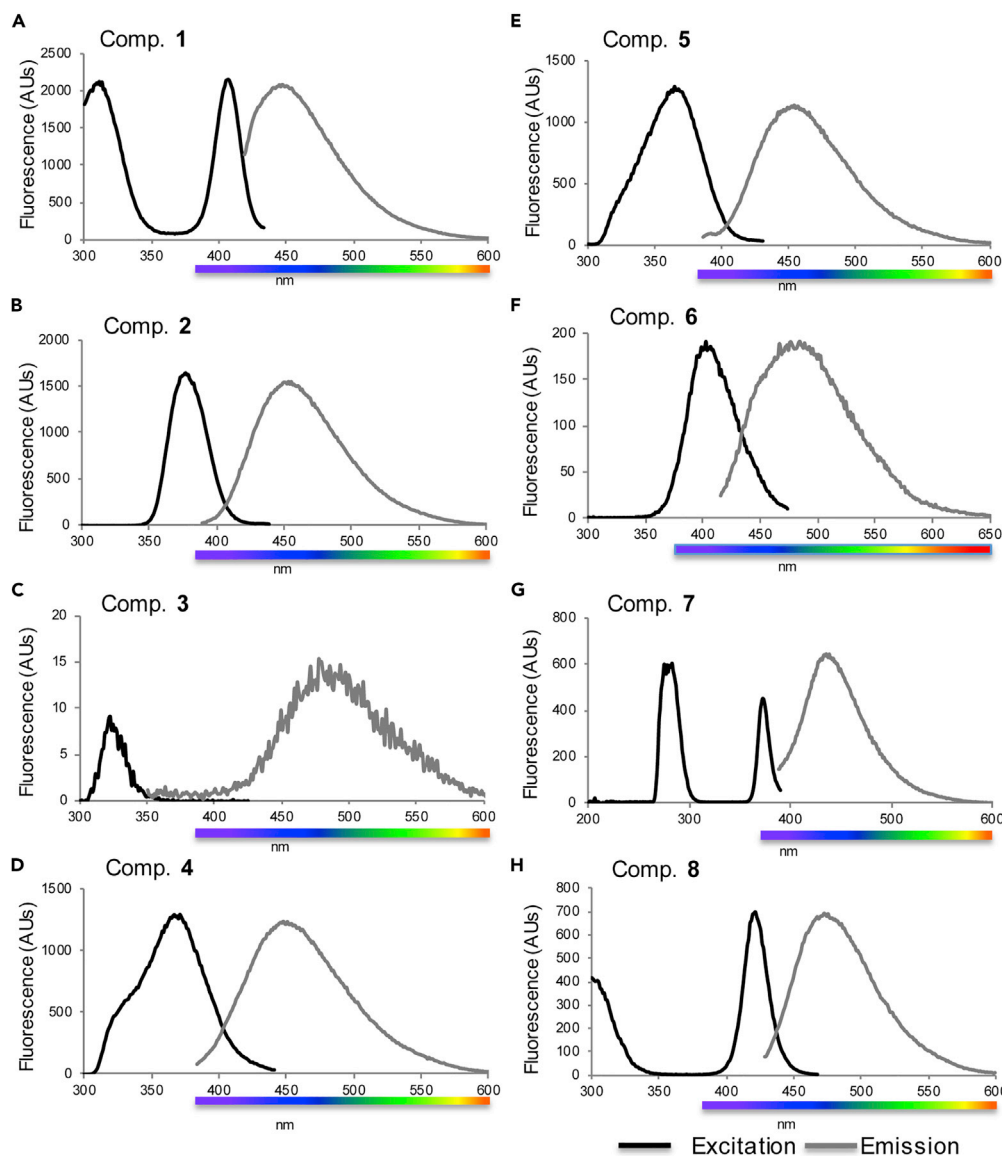
Figure 5. Absorbance and Fluorescence Emission of Shark Skin Metabolites

(A–H) Fluorescence Spectra of Pure Compounds **1**–**8** in methanol. See Figure S20 for spectra in PBS.

methanol revealed a blue wavelength emission maximum of 472 nm (Figure 5H). Given the discrepancy, we further obtained fluorescence spectra of the compounds in a more biologically relevant phosphate buffered saline (PBS) system, and the compounds displayed significant shifts of their fluorescence spectra compared with those in methanol (Table 1 and Figure S20). Specifically, the fluorescence emission spectrum of **8** exhibited a green emission maximum of 507 nm (Table 1 and Figure S20H). Consistent with kynurenine yellow, a large Stokes shift was observed in **8**, which is known to be derived from a charge transfer from the amino group to the carbonyl group in the kynurenine yellow scaffold (Zelentsova et al., 2013). Thus, bromo-tryptophan-kynurenine metabolism products in an aqueous environment represent the chemical source of bright green biofluorescence in shark skins.

Antibacterial Activities of the Metabolites

Collectively, we structurally characterized the previously undescribed chemical source of green-dominated biofluorescence in the skin of both sharks (Figure 6). In the marine environment, *C. ventriosum* is benthic

iScience

CellPress

	Methanol		PBS	
	Excitation Max (nm)	Emission Max (nm)	Excitation Max (nm)	Emission Max (nm)
Compound **1**	407	447	414	451
Compound **2**	370	453	401	481
Compound **3**	323	477	NA[a]	NA[a]
Compound **4**	370	448	360	400
Compound **5**	370	454	363	465
Compound **6**	403	484	388	495
Compound **7**	374	439	360	420
Compound **8**	422	472	438	507

Table 1. Fluorescence of Compounds in Methanol and PBS
[a]Not applicable due to low solubility.

(bottom-dwelling) and predominantly remains in direct contact with underwater sediment. Figures S21 and S22 show the demersal habitat of *C. ventriosum* from Scripps Canyon, California. As marine sediments have higher concentrations of bacteria than the water column (Karl and Novitsky, 1988), we evaluated the antibacterial activities of metabolites **1–7** against two bacterial pathogens, including a Gram-positive methicillin-resistant *Staphylococcus aureus* (MRSA) and a Gram-negative *Vibrio parahaemolyticus*. *V. parahaemolyticus* was chosen as a candidate as it is a common marine bacterium, often found in sediment. Major compound **4** found in both light and dark skin tissue samples exhibited a half-maximal inhibitory concentration (IC_{50}) value of 66 μM against MRSA, and compound **3** showed growth inhibitory activity against *V. parahaemolyticus* at an IC_{50} of 14 μM. The other metabolites showed no significant activity at concentrations up to 100 μM (Figures S23 and S24). Based on these observations, the antibacterial properties of these biofluorescent metabolites may thus also contribute in part to chemical defense against microbial pathogens in the marine environment.

DISCUSSION

Although biofluorescence is a fascinating phenomenon that has been reported in an increasing diversity of marine species in recent years, including sharks (Gruber et al., 2016; Sparks et al., 2014) and sea turtles (Gruber and Sparks, 2015), its molecular origins remain largely unexplored. In this study, we describe a family of natural small molecule fluorophores that significantly contribute to shark skin biofluorescence. Interestingly, these small molecule metabolites represent a parallel bromo-tryptophan-kynurenine biosynthetic pathway to that of the established tryptophan-kynurenine pathway widely found in vertebrates (Cervenka et al., 2017). For example, kynurenine and its analogs regulate diverse human biological processes, and accumulation of kynurenine in the brain is tightly associated with mental health disorders such as depression and schizophrenia (Cervenka et al., 2017). Of note, a halogenated kynurenine, L-4-chloro-kynurenine, is a neuro-pharmaceutical prodrug of 7-chlorokynurenic acid, used to treat major depressive disorder (Véc-sei et al., 2012). Although potential neurological activities of the brominated variant **1** and its analogs remain an open question, it is intriguing to find brominated variants of mammalian signaling molecules in shark skin. Although the exact source of the halogenase and its bromo-tryptophan product (whether it be of shark, microbial symbiont, or environmental origin) remain unresolved, the observed diversity of bromo-tryptophan catabolic processing in *E. coli* suggests that similarly flexible metabolic pathways may also be at play in shark skin. As we observed differential regulation of these metabolites in light versus dark skin, future studies aimed at assessing whether tryptophan-kynurenine metabolism genes are similarly regulated, are warranted. Analogous to non-brominated kynurenine molecules functioning as UV radiation filters in the human lens, these brominated kynurenine molecules could, in principle, complement melanin pigments within shark skin to offer photo-protection from low-wavelength light (Sweet et al., 2012; Taylor et al., 2002). Collectively, the discovery of brominated tryptophan-kynurenine metabolism products from marine shark skins in our study not only illuminates the likely source of naturally occurring biofluorescence of shark skins but also raises new questions regarding their potential roles in central nervous system signaling, the resilience of shark skins to microbial infections, and diverse skin pigmentation phenotypes.
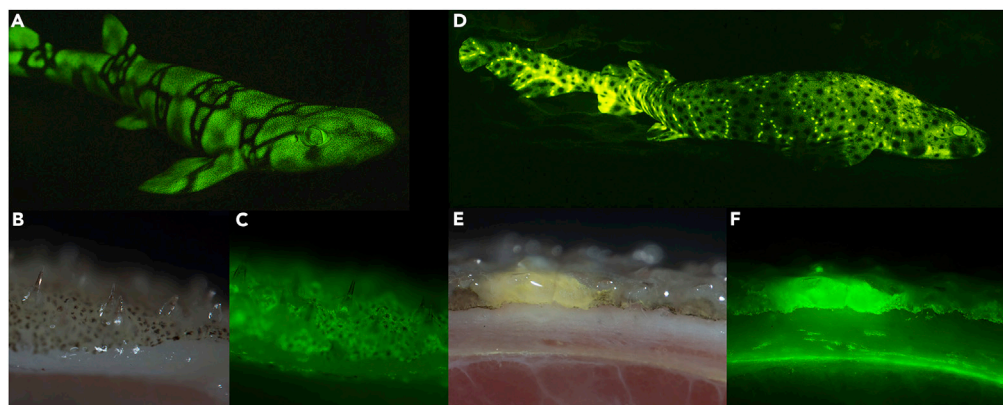
Figure 6. Cross-Section of Sharks Showing Localization of Fluorescence in Skin Tissue

(A) *Scyliorhinus retifer* excited with 450–500 nm and imaged through 514nmLP, (B) cross section of skin with white light; (C) fluorescence emission, (D) *Cephaloscyllium ventriosum* excited with 450–500 nm and imaged through 514nmLP, (E) cross section of skin with white light, (F) fluorescence emission.

Limitations of the Study

A wide range of marine organisms are known to be biofluorescent, but the chemical ecological contributions to naturally occurring biofluorescence phenotypes has not been investigated at the detailed molecular level. As representative marine vertebrate animals, we focused on elucidating the bright green biofluorescence phenotype in swell sharks and in chain catsharks. A bromo-tryptophan precursor and a bromo-diketopiperazine antibiotic were found in both skin types, whereas in light skin, the bromo-tryptophan precursor was processed through the kynurenine metabolic pathway, generating a collection of brominated metabolites with varying spectral properties. Although we focused on the characterization of small molecule sources involved in shark biofluorescence phenotypes in this study, underlying biosynthesis of these metabolites still remains to be explored. As aqueous sodium hydroxide was the solvent used for extraction of shark skin materials in our system, we cannot rule out the possibility that the small molecule fluorophores derive from base-catalyzed ester hydrolysis of currently uncharacterized parent molecules. However, pure bromo-tryptophan as a standard solubilized under basic conditions and precipitated under acidic conditions (Figure S25), consistent with our small molecule findings.

METHODS

All methods can be found in the accompanying Transparent Methods supplemental file.

SUPPLEMENTAL INFORMATION

Supplemental Information can be found online at https://doi.org/10.1016/j.isci.2019.07.019.

AUTHOR CONTRIBUTIONS

H.B.P., D.F.G., and J.M.C conceived and designed the experiments. H.B.P and Y.C.L. carried out the analytical isolation and analysis, chemical synthesis, and structural characterization of metabolites. J.P.G. and S.R.K. obtained the fluorescence spectra of metabolites. J.C.W. performed fluorescent microscopy of sharks. D.F.G. performed *in situ* underwater fluorescent imagery of sharks. V.P. designed or engineered underwater fluorescent lamps. R.H. isolated bromo-kynurenine. H.B.P, J.P.G., D.F.G., and J.M.C wrote the manuscript. All authors reviewed and edited the manuscript.

iScience

CellPress

DECLARATION OF INTERESTS

The authors declare that no competing interests.

REFERENCES

Bortolotti, P., Hennart, B., Thieffry, C., Jausions, G., Faure, E., Grandjean, T., Thepaut, M., Dessein, R., Allorge, D., Guery, B.P., et al. (2016). Tryptophan catabolism in *Pseudomonas aeruginosa* and potential for inter-kingdom relationship. BMC Microbiol. *16*, 137.

Castro, J.I. (2011). The Sharks of North America (Oxford University Press).

Cervenka, I., Agudelo, L.Z., and Ruas, J.L. (2017). Kynurenines: tryptophan's metabolites in exercise, inflammation, and mental health. Science *357*, eaaf9794.

Chalfie, M., Tu, Y., Euskirchen, G., Ward, W.W., and Prasher, D.C. (1994). Green fluorescent protein as a marker for gene expression. Science *263*, 802–805.

Claes, J.M., Dean, M.N., Nilsson, D.E., Hart, N.S., and Mallefet, J. (2013). A deepwater fish with 'lightsabers'–dorsal spine-associated luminescence in a counterilluminating lanternshark. Sci. Rep. *3*, 1308.

Compagno, L.J.V. (1984). FAO species catalogue. In Sharks of the world: an annotated and illustrated catalogue of shark species known to date. FAO Fish Synop 125, *Vol. 4*, (Food and Agriculture Organization of the United Nations), pp. 251–655.

Deheyn, D.D., Kubokawa, K., McCarthy, J.K., Murakami, A., Porrachia, M., Rouse, G.W., and Holland, N.D. (2007). Endogenous green fluorescent protein (GFP) in amphioxus. Biol. Bull. *213*, 95–100.

Forouhar, F., Anderson, J.L.R., Mowat, C.G., Vorobiev, S.M., Hussain, A., Abashidze, M., Bruckmann, C., Thackray, S.J., Seetharaman, J., Tucker, T., et al. (2007). Molecular insights into substrate recognition and catalysis by tryptophan 2,3-dioxygenase. Proc. Natl. Acad. Sci. U S A *104*, 473–478.

Gruber, D.F., Gaffney, J.P., Mehr, S., DeSalle, R., Sparks, J.S., Platisa, J., and Pieribone, V.A. (2015). Adaptive evolution of eel fluorescent proteins from fatty acid binding proteins produces bright fluorescence in the marine environment. PLoS One *10*, e0140972.

Gruber, D.F., Kao, H.-T., Janoschka, S., Tsai, J., and Pieribone, V.A. (2008). Patterns of fluorescent protein expression in scleractinian corals. Biol. Bull. *215*, 143–154.

Gruber, D.F., Loew, E.R., Deheyn, D.D., Akkaynak, D., Gaffney, J.P., Smith, W.L., Davis, M.P., Stern, J.H., Pieribone, V.A., and Sparks, J.S. (2016).

Biofluorescence in catsharks (Scyliorhinidae): Fundamental description and relevance for elasmobranch visual ecology. Sci. Rep. *6*, 24751.

Gruber, D.F., and Pieribone, V.A. (2006). Aglow in the Dark: The Revolutionary Science of Biofluorescence (Belknap Press of Harvard University Press), p. 288.

Gruber, D.F., and Sparks, J.S. (2015). First observation of fluorescence in marine turtles. Am. Mus. Novit. *3845*, 1–8.

Hayashi, S., and Toda, Y. (2009). A novel fluorescent protein purified from eel muscle. Fish. Sci. *75*, 1461.

Higgins, R.C., Townsend, N.O., and Jackson, Y.A. (2009). Benzylic oxidation of N-acyl-1,2,3,4-tetrahydroquinolines. Heterocycles *78*, 3011–3021.

Karl, D.M., and Novitsky, J.A. (1988). Dynamics of microbial growth in surface layers of a coastal marine sediment ecosystem. Mar. Ecol. Prog. Ser. *50*, 169–176.

Kolodziej, L.R., Paleolog, E.M., and Williams, R.O. (2011). Kynurenine metabolism in health and disease. Amino Acids *41*, 1173–1183.

Kumagai, A., Ando, R., Miyatake, H., Greimel, P., Kobayashi, T., Hirabayashi, Y., Shimogori, T., and Miyawaki, A. (2013). A bilirubin-inducible fluorescent protein from eel muscle. Cell *153*, 1602–1611.

Kurnasov, O., Jablonski, L., Polanuyer, B., Dorrestein, P., Begley, T., and Osterman, A. (2003). Aerobic tryptophan degradation pathway in bacteria: novel kynurenine formamidase. FEMS Microbiol. Lett. *227*, 219–227.

Matz, M.V., Fradkov, A.F., Labas, Y.A., Savitsky, A.P., Zaraisky, A.G., Markelov, M.L., and Lukyanov, S.A. (1999). Fluorescent proteins from nonbioluminescent Anthozoa species. Nat. Biotechnol. *17*, 969–973.

Mazarei, G., and Leavitt, B.R. (2015). Indoleamine 2,3 dioxygenase as a potential therapeutic target in Huntington's disease. J. Huntingtons Dis. *4*, 109–118.

Meyers, A., Fradkov, A.F., Shagin, D.A., Widder, E.A., Barsova, E.V., Nunez, J.M., Ugalde, J.A., Lukyanov, K.A., Matz, M.V., Lukyanov, S.A., et al. (2004). GFP-like proteins as ubiquitous metazoan superfamily: evolution of functional features and structural complexity. Mol. Biol. Evol. *21*, 841–850.

Mizdrak, J., Hains, P.G., Kalinowski, D., Truscott, R.J.W., Davies, M.J., and Jamie, J.F. (2007). Novel human lens metabolites from normal and cataractous human lenses. Tetrahedron *63*, 4990–4999.

Schnepel, C., Minges, H., Frese, M., and Sewald, N. (2016). A high-throughput fluorescence assay to determine the activity of tryptophan halogenases. Angew. Chem. Int. Ed. *55*, 14159–14163.

Shagin, D.A., Barsova, E.V., Yanushevich, Y.G., Fradkov, A.F., Lukyanov, K.A., Labas, Y.A., Semenova, T.N., Ugalde, J.A., Meyers, A., Nunez, J.M., et al. (2004). GFP-like proteins as ubiquitous metazoan superfamily: evolution of functional features and structural complexity. Mol. Biol. Evol. *21*, 841–850.

Shimomura, O., Johnson, F.H., and Saiga, Y. (1962). Extraction, purification and properties of aequorin, a bioluminescent protein from the luminous hydromedusan, *Aequorea*. J. Cell. Comp. Physiol. *59*, 223–239.

Sparks, J.S., Schelly, R.C., Smith, W.L., Davis, M.P., Tchernov, D., Pieribone, V.A., and Gruber, D.F. (2014). The covert world of fish biofluorescence: a phylogenetically widespread and phenotypically variable phenomenon. PLoS One *9*, e83259.

Sweet, M., Kirkham, N., Bendall, M., Currey, L., Bythell, J., and Heupel, M. (2012). Evidence of melanoma in wild marine fish populations. PLoS One *7*, e41989.

Taylor, L.M., Andrew Aquilina, J., Jamie, J.F., and Truscott, R.J.W. (2002). UV filter instability: consequences for the human lens. Exp. Eye Res. *75*, 165–175.

Tsien, R.Y. (1998). The green fluorescent protein. Annu. Rev. Biochem. *67*, 509–544.

Van der Leek, A.P., Yanishevsky, Y., and Kozyrskyj, A.L. (2017). The kynurenine pathway as a novel link between allergy and the gut microbiome. Front. Immunol. *8*, 1374.

Vécsei, L., Szalárdy, L., Fülöp, F., and Toldi, J. (2012). Kynurenines in the CNS: recent advances and new questions. Nat. Rev. Drug Discov. *12*, 64–82.

Zelentsova, E.A., Sherin, P.S., Snytnikova, O.A., Kaptein, R., Vauthey, E., and Tsentalovich, Y.P. (2013). Photochemistry of aqueous solutions of kynurenic acid and kynurenine yellow. Photochem. Photobiol. Sci. *12*, 546–558.

Supplemental Information

Bright Green Biofluorescence in Sharks

Derives from Bromo-Kynurenine Metabolism

Hyun Bong Park, Yick Chong Lam, Jean P. Gaffney, James C. Weaver, Sara Rose Krivoshik, Randy Hamchand, Vincent Pieribone, David F. Gruber, and Jason M. Crawford

Transparent Methods

General

¹H and 2D (gCOSY, gHSQCAD, and gHMBCAD) NMR spectra were obtained from an Agilent 600 MHz spectrometer with a cold probe (Agilent, Santa Clara, CA, USA) in methanol-d_4 (Cambridge Isotope Laboratories, Inc. Tewksbury, MA, USA). High-resolution (HR) ESI-QTOF-MS data were recorded using an Agilent iFunnel 6550 system with a Phenomenex Kinetex C_{18} (100 Å) 5 μm (250 × 4.6 mm) column. For general HR-ESI-QTOF-MS analysis, extracts were prepared by resuspension in 100 μl methanol (LC-MS grade, Fisher, USA). 2 μl of samples were injected and analyzed at 25 ºC and 0.7 ml/min with a water:acetonitrile gradient solvent system containing 0.1% formic acid: 0-30 min, 10-100% acetonitrile; hold for 5 min, 100% acetonitrile; 2 min, 100-10% acetonitrile; 5 min equilibration time 10% acetonitrile. Mass spectra were acquired in the range of 25-1700 *m/z* in positive ion mode. Collected data was analyzed using Agilent MassHunter Qualitative Analysis Software (Version B.06.00, Agilent Technologies), and all targeted mass ions were extracted and analyzed within a 10 ppm error range [extracted ion count (EIC) chromatograms]. Sep-Pak® Vac 35 cc (10 g) C_{18} cartridge (Waters Corporation, Milford, MA) was used for the flash column chromatography. Reversed-Phase High-Performance Liquid Chromatography (RP-HPLC) was performed on an Agilent Prepstar HPLC system. Two reversed-phase columns, an Agilent Polaris C18-A 5 μm (250 × 21.2 mm) column and a Phenomenex Luna C_{18}(2) (100 Å) 10 μm (250 × 10.0 mm) column, were used for the separation and purification of metabolites, respectively. Routine low-resolution HPLC-MS analysis was acquired by using an Agilent 1260 Infinity Quaternary LC system with an autosampler and a photo diode array (PDA) detector coupled to an Agilent 6120 single quadrupole Electrospray Ionization (ESI) mass spectrometer.

Shark skin collection and extraction

Specimens of *Cephaloscyllium ventriosum* were obtained from Marinus Scientific, LLC. This study was approved and carried out in strict accordance with the recommendations in the Guidelines for the Use of Fishes in Research of the American Fisheries Society and the John B. Pierce Laboratory's Institutional Animal Care and Use Committee (IACUC) # VP5-2019. The *Scyliorhinus retifer* skin used in this study was from Gruber et al (2016). A small fragment of the fluorescent skin of each shark species was dissected and used for extraction studies. As the fluorescent molecules are soluble in 0.1 M sodium hydroxide, samples of the shark were cut in 1 cm x 1 cm pieces and allowed to incubate in 0.1 M sodium hydroxide for 1 h before experiments were conducted. Fluorescence spectra of shark skin extracts were recorded on a Hitachi F-7000 Fluorimeter.

Larger-scale extraction and isolation of metabolites

Crude materials from skin of the swell shark were extracted in a 0.1 M sodium hydroxide solution, followed by subsequent extraction of the small molecule fraction with butanol. The small molecules were fractionated by reversed-phase analytical HPLC system, eluting 30 HPLC fractions using a Phenomenex Kinetex C_{18} (2) 5 μm column (250 × 4.6 mm) with a gradient of 0.01% trifluoroacetic acid in acetonitrile/water (Flow rate: 1 ml/min; 0-60 min, 10/90→100/0%, 1 min fraction window). HPLC fraction 12 was further subjected to reversed-phase HPLC [Column: Phenomenex Luna C_{18} (100Å) 10 μm (250 × 4.6 mm)] with a linear gradient in acetonitrile/water mobile phase elution (Flow rate: 1 ml/min; 0-60 min, 10/90→100/0%) to yield a 6-bromo-tryptophan (**5**) (t_R = 10.5 min). The butanol-soluble fraction was subjected to a Sep-Pak® Vac 35 cc (10 g) C_{18} cartridge with a step gradient elution (20%, 40%, 60%, 80%, and 100% methanol in water). The 80% methanol fraction was further fractionated using an Agilent Prepstar HPLC system [Agilent Polaris C_{18}-A 5 μm (250 × 21.2 mm) column] with a linear gradient elution (50-100% acetonitrile in water over 60 min, 8 ml/min, 1 min fraction collection window). The HPLC fraction 18 was purified on an Agilent Phenyl-Hexyl 5 μm (250 × 9.4 mm) column using a linear gradient separation (50-100% acetonitrile in water, 2 ml/min) to yield 6-bromo-DKP (**4**) (t_R = 10.1 min). The purified compounds were dried under reduced pressure on a Genevac HT-4X system over 12 h for NMR analysis. All chemical structures of materials were fully characterized by LC-MS co-injection with standards, 2D-NMR, and MS analysis.

Chemical synthesis of metabolites

6-Bromo-DL-tryptophan was purchased from Santa Cruz Biotechnology (Dallas, TX, USA). To synthesize 8-bromo-DL-*N*-formyl-kynurenine, 6-bromo-DL-tryptophan (50 mg, 0.177 mmol, 1.0 eq) was added to a 10 ml round-bottom flask under air atmosphere. The chemical was suspended in 2 ml water and *meta*-chloroperoxybenzoic acid (0.32 g, 1.854 mmol, 10.5 eq) was subsequently added. The reaction was stirred at room temperature under air atmosphere for 20 h and completion of the reaction was monitored by LC-MS analysis. Upon completion, the reaction was transferred to a 20 ml scintillation vial using methanol and completely dried down using nitrogen gas. The reaction material was fractionated on a Sep-Pak® Vac 35 cc (10 g) C_{18} cartridge with a step gradient elution (20, 40, and 60% methanol in water). The 40% methanol fraction containing 8-bromo-DL-*N*-formyl-kynurenine (t_R = 22.4 min, 3 mg) was then purified using a reversed-phase HPLC with a Phenomenex Luna C_{18} (100Å) 10 μm column (250 × 4.6 mm) and a gradient of 20% to 80% aqueous methanol for 30 min with a flow rate of 2 ml/min. For the deformylation, 8-bromo-DL-*N*-formyl-kynurenine (2 mg, 0.006 mmol, 1.0 eq) was dissolved in a 1:1 mixture of trifluoroacetic acid:water (600 μl). The reaction was stirred for 4 h at room temperature and dried using nitrogen

gas. The 8-bromo-DL-kynurenine (t_R = 24.3 min, 2 mg) was then isolated on a Phenomenex Luna C$_{18}$ (100Å) 10 µm column (250 × 4.6 mm) at a flow rate of 2 ml/min with a linear gradient from 10%-80% over 30 min. Syntheses of enantiopure 8-bromo-L-*N*-formyl-kynurenine (**2**) and 8-bromo-L-kynurenine (**1**) were conducted as above, but with using enantiopure 6-bromo-L-tryptophan (**5**) as starting material. For the deamination, 8-bromo-DL-kynurenine (2 mg) was dissolved in anhydrous dimethylformamide (1 ml) and the reaction was initiated at 70 °C and completed after 3 h. The reaction mixture was dried and was purified by reversed-phase HPLC [Phenomenex Luna C$_{18}$ (100Å) 10 µm column (250 × 4.6 mm), 2 ml/min] with a linear gradient of 10% acetonitrile/0.1% formic acid-100% acetonitrile/0.1% formic acid in water over 60 min with a flow rate of 2 ml/min to yield 8-bromo-CKA (carboxyketoalkene) (**3**) (t_R = 36.1 min, 0.6 mg).

For the chemical synthesis of compound **8**, 7-bromoquinoline-2-carboxylic acid (**8a**) was purchased from Millipore Sigma (St. Louis, MO, USA). Compound **8a** (200 mg) was suspended in a solvent mixture (acetone/water = 10:1). Methyl iodide (300 µl) and potassium carbonate (600 mg) were added and refluxed for 2 h. The reaction mixture was dried and extracted with ethyl acetate to yield **8b** (~200 mg). Reduction of **8b** in glacial acetic acid (5 ml) was performed utilizing sodium cyanoborohydride (150 mg) at 25 °C for 3 h. The reaction mixture was neutralized with saturated sodium bicarbonate followed by the ethyl acetate extraction twice. The crude reaction materials were directly treated with acetic anhydride (8 ml) and heated at 90 °C for 3 h and was separated by reversed-phase HPLC [Phenomenex Luna C$_{18}$ (100Å) 10 µm column (250 × 4.6 mm), 2 ml/min] with a linear gradient of 20% acetonitrile/0.1% formic acid-60% acetonitrile/0.1% formic acid in water for 30 min with a flow rate of 2 ml/min to yield **8d** (t_R = 16.2 min, 110 mg). The benzylic oxidation on **8d** (80 mg) was initiated with chromium hexacarbonyl (50 mg) and *tert*-butyl hydroperoxide (70 wt% in water, 600 µl) in acetonitrile and refluxed for 24 h. The product **8e** was eluted at t_R = 16.5 min under the aforementioned purification condition for **8d**. The deprotection of **8e** (15 mg) was achieved in water containing potassium carbonate (20 mg) and refluxed for 2 h, yielding **8** (13 mg).

Biotransformation of 6-bromo-tryptophan to 8-bromo-kynurenine in *E. coli*

E. coli Nissle 1917 (EcN) colonies were used to inoculate 5 ml of lysogeny broth (LB) (BD, Franklin Lakes, NJ, USA; 1% (w/v) tryptone, 0.5% (w/v) yeast extract, and 1% (w/v) sodium chloride) for a total of three biological replicates and incubated at 37 °C with shaking at 250 rpm for 16 h. After overnight, 20 µl of each seed culture was used to inoculate 2 ml of M9 minimal medium (VWR Funding Inc., West Chester, PA, USA; 0.6% (w/v) Na$_2$HPO$_4$, 0.3% (w/v) KH$_2$PO$_4$, 0.05% (w/v) NaCl, 0.1% (w/v) NH$_4$Cl, 0.2% (w/v) glucose, 2 mM MgSO$_4$, and 0.1 mM CaCl$_2$)

supplemented with 10 mM 6-bromo-D-tryptophan, 10 mM 6-bromo-L-tryptophan, 1 mM 6-bromo-D-tryptophan, 1 mM 6-bromo-L-tryptophan, or nothing (negative control). The inoculated cultures were grown at 37 °C with shaking at 250 rpm. After 20 h cultivation, each culture was extracted with 3 ml butanol, vortexed, and centrifuged. The organic layers were dried and resuspended in 80 µl methanol for LC-MS analysis. These experiments were performed with biological triplicates. Addition of the amino acids required solubilization in 1N sodium hydroxide, followed by neutralization with 1N hydrochloric acid.

Fluorescence spectra

Fluorescence spectra from all compounds **1**-**8** were measured at a concentration of 5 mM in methanol on a Hitachi-F-7000 Spectrophotometer.

***In situ* and microscope fluorescence imaging**

To excite a fluorescence response of the sharks, a Aquatica Rouge underwater housing was fitted with custom designed blue excitation lighting. The LED light (Royal Blue) was collimated to ensure its perpendicular incidence on the scientific grade 450/70 nm interference filter surface (Semrock, Inc., Lake Forest, IL), minimizing the transmission of out-of-band energy. The ultra-bright LEDs, collimating lenses, filters, and exit diffusers were contained in custom-made water- and pressure-proof housings and powered by NiMH Battery Packs (Ikelite Underwater Systems, Indianapolis, IN). To image and record biofluorescence, a scientific-grade 514 nm long-pass emission filter (Semrock, Inc.) was placed in front of the sensor of the camera. Cross-sections of both sharks were taken on an AxioZoom v16 stereo fluorescent microscope using a PlanNeoFluar Z 2.3×/0.57 objective and 38 HE GFP filter set.

Marfey's analysis for absolute configuration determination

Dried 6-bromo-DKP (diketopiperazine) (**4**) (~0.1 mg) was acid-hydrolyzed in 1 N hydrochloric acid (250 µl) at 110 °C for 1 h with stirring. After cooling down, the hydrolysate was dried under the purge of nitrogen gas. The standards D- and L-6-bromo-tryptophan were purchased from LabNetwork, Inc. (South Portland, ME, USA). The standards D- and L-8-bromo-kynurenines and 8-bromo-*N*-formyl-kynurenines were prepared as described in the chemical synthesis section. The dried hydrolysates, naturally-purified compounds, and commercial standards, were treated with 25 µl of a solution of N_α-(2,4-dinitro-5-fluorophenyl)-L-alaninamide (FDAA) (10 mg/ml in acetone) followed by the addition of 100 µl of 1 N sodium bicarbonate to yield L-FDAA derivatized compounds. The reactions were heated at 80 °C for 3 min and neutralized with 25 µl of 2 N hydrochloric acid. The Marfey's derivatives were then diluted to 20-100 µl methanol for single quadrouple LC-MS and/or HR-ESI-QTOF-MS analysis. 2-10 µl

samples were analyzed using a Phenomenex Kinetex C_{18} (100Å) 5 µm (250 × 4.6 mm) column with a flow rate (0.7 ml/min) and a solvent system of water and acetonitrile containing 0.1% formic acid (v/v). The retention times of L-FDAA derivatized compounds were determined as follows: a linear gradient elution with 50-100% acetonitrile, 6.2 min for L-FDAA derivatized 6-bromo- L-tryptophan, 6.8 min for L-FDAA derivatized 6-bromo-D-tryptophan, 6.5 min for L-FDAA derivatized 8-bromo- L-kynurenine, and 7.1 min for L-FDAA derivatized 8-bromo-D-kynurenine.

Antibacterial activity of metabolites

Antibacterial activities of metabolites were evaluated using the minimum inhibitory concentration (MIC) assay in 96-well plates. Stock solutions of metabolites were prepared in sterile dimethyl sulfoxide with a concentration of 10 mM. Dimethyl sulfoxide was used as a negative control, and chloramphenicol was prepared as positive control for the antibacterial activity against methicillin-resistant *Staphylococcus aureus* (MRSA) and *Vibrio parahaemolyticus*. The stock solutions of compounds (10 mM) were serially diluted and adjusted to ten different final concentrations (100, 50, 25, 12.5, 6.25, 3.13, 1.56, 0.78, 0.39, and 0.19 µM) in the same concentration of fresh dimethyl sulfoxide. MRSA was grown in tryptic soy broth (TSB) and *V. parahaemolyticus* was grown in Marine Broth. Media (50 µl) containing compound at the varying concentrations was added to each well. Overnight cultures of the bacteria were diluted to OD_{600} = 0.05, 50 µl of the cell culture broth was then dispensed into individual wells, and the plates were sealed and incubated at 37 °C overnight. Plates were then read for OD_{600} using a PerkinElmer Envision 2100 multimode plate reader (PerkinElmer, Waltham, MA, USA). All samples were tested in triplicate.
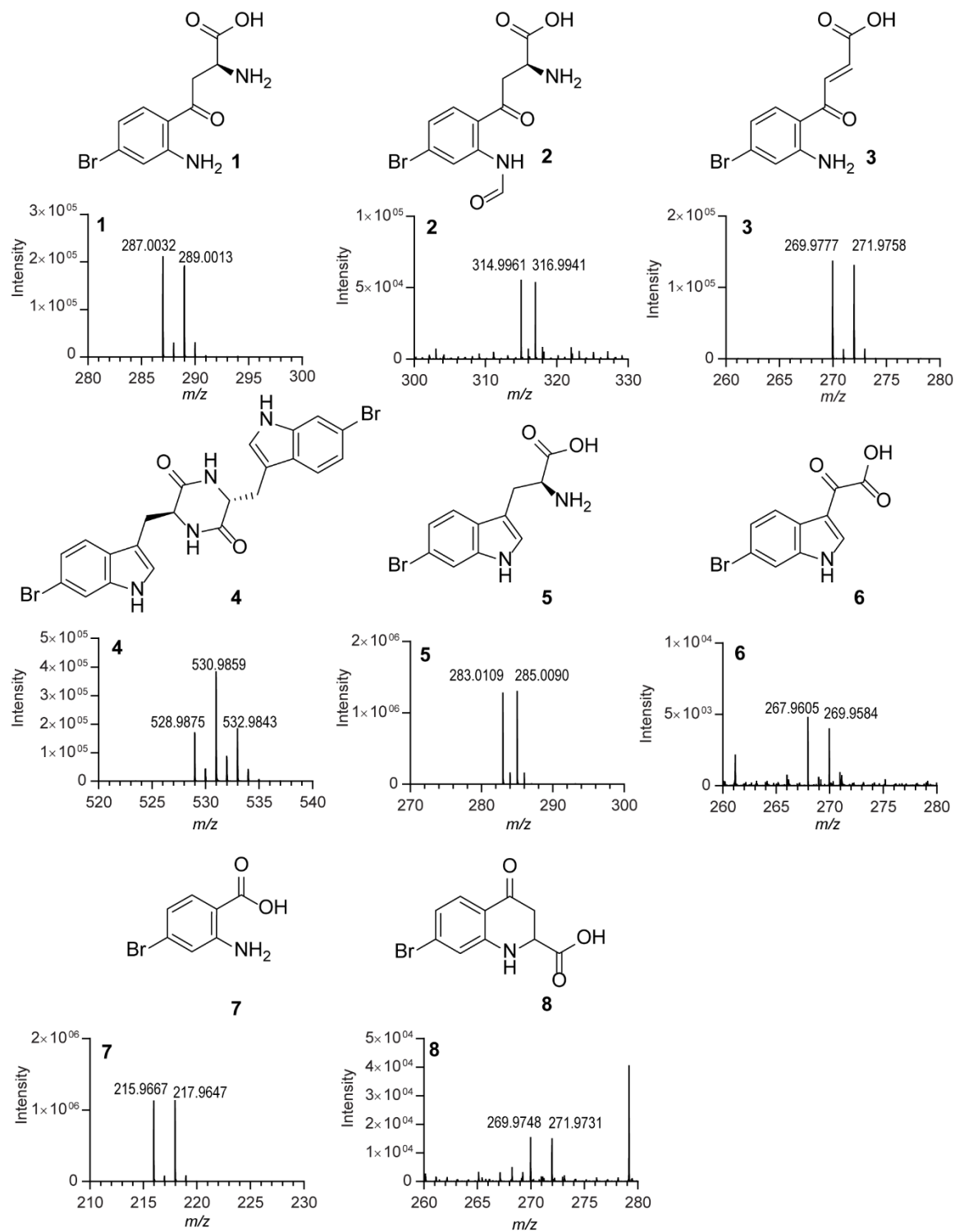
Figure S1. HR-ESI-QTOF-MS spectra of metabolites **1-8**. Related to Figure 2.
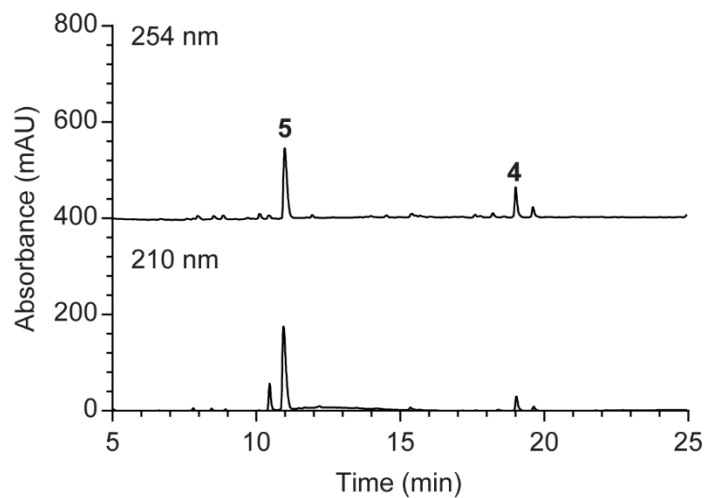
Figure S2. HPLC chromatogram of crude extract from the skin of *C. ventriosum*. The 10 mg of crude samples were dissolved in 100 μl methanol and 10 μl of samples were analyzed for HPLC-MS analysis. This figure shows the two major metabolites, **4** and **5** (210 and 254 nm spectra are shown). Related to Figure 2.
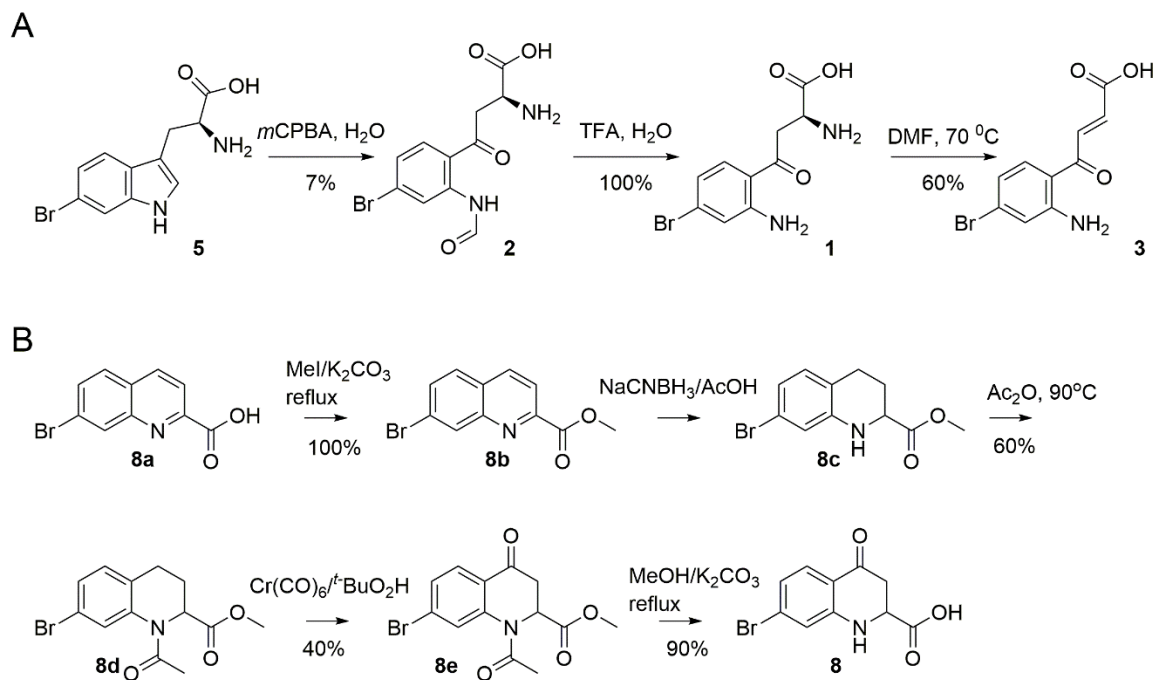
**Figure S3.** Synthetic scheme of metabolites **1**-**3** (A) and **8** (B). Related to Figure 2.
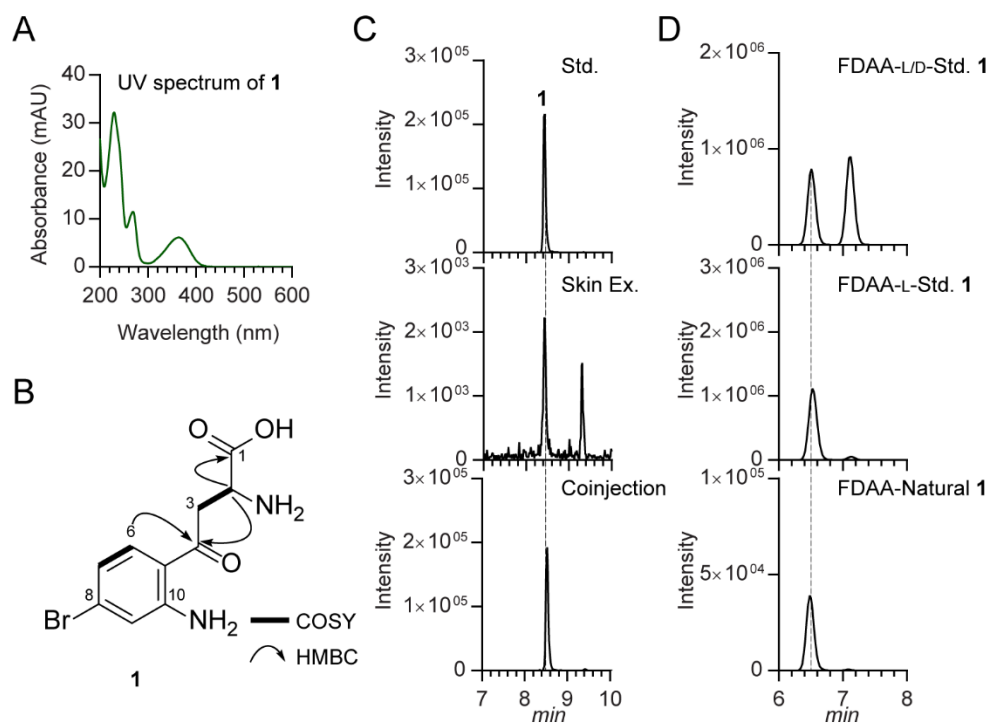
Figure S4. Structural characterization of **1**. (A) UV-visible spectrum of purified **1**. (B) Key 2D NMR (COSY and HMBC) correlations of **1**. (C) Co-injection studies using skin extract and standard **1**. (D) Marfey's analysis. Related to Figure 2.
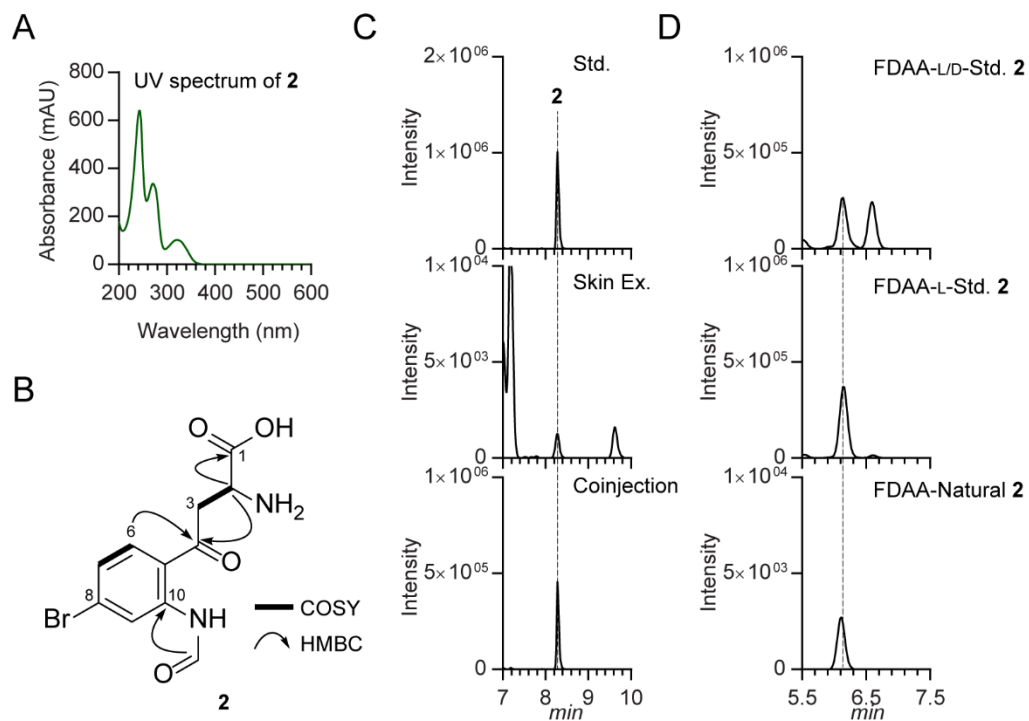
Figure S5. Structural characterization of **2**. (A) UV-visible spectrum of purified **2**. (B) Key 2D NMR (COSY and HMBC) correlations of **2**. (C) Co-injection with skin extract and standard **2**. (D) Marfey's analysis. Related to Figure 2.
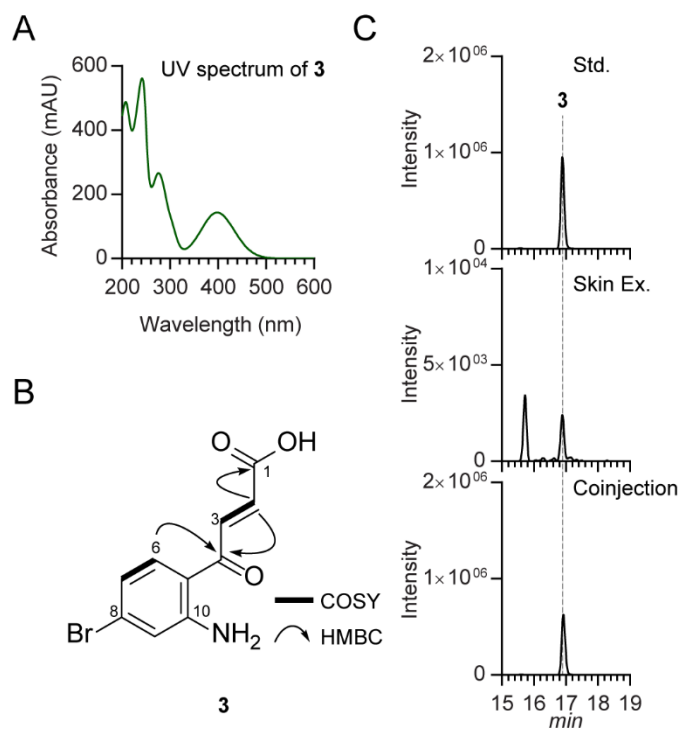
Figure S6. Structural characterization of **3**. (A) UV-visible spectrum of purified **3**. (B) Key 2D NMR (COSY and HMBC) correlations of **3**. (C) Co-injection with skin extract and standard **3**. Related to Figure 2.
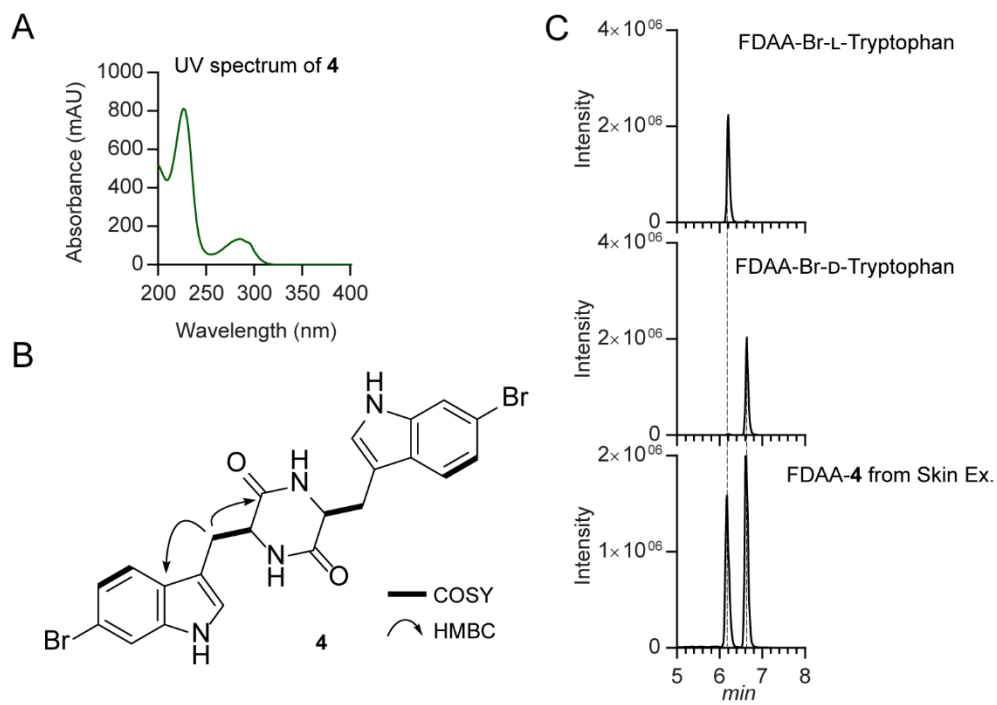
**Figure S7.** Structural characterization of **4**. (A) UV-visible spectrum of purified **4**. (B) Key 2D NMR (COSY and HMBC) correlations of **4**. (C) Marfey's analysis. Related to Figure 2.
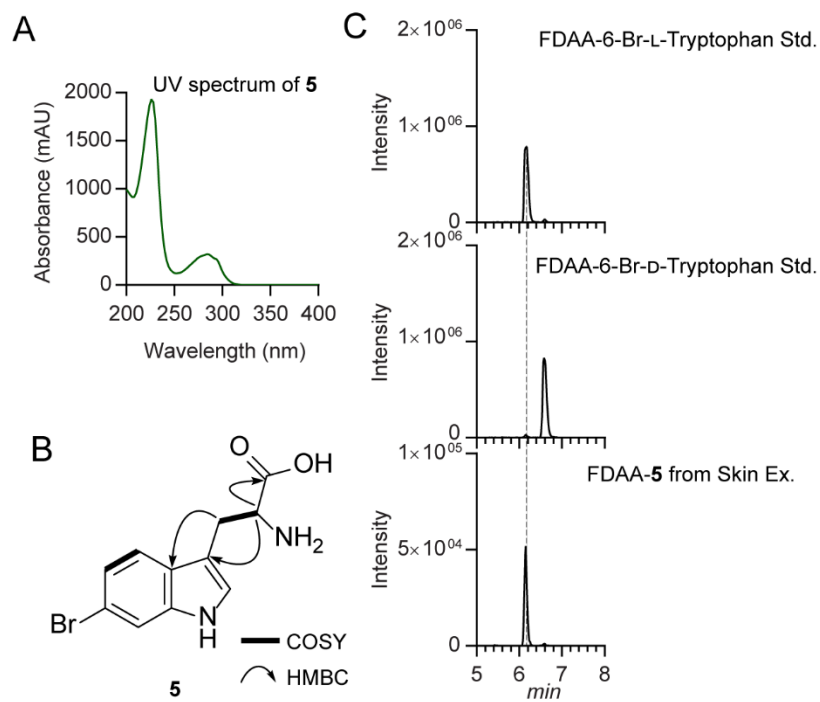
Figure S8. Structural characterization of **5**. (A) UV-visible spectrum of purified **5**. (B) Key 2D NMR (COSY and HMBC) correlations of **5**. (C) Marfey's analysis. Related to Figure 2.
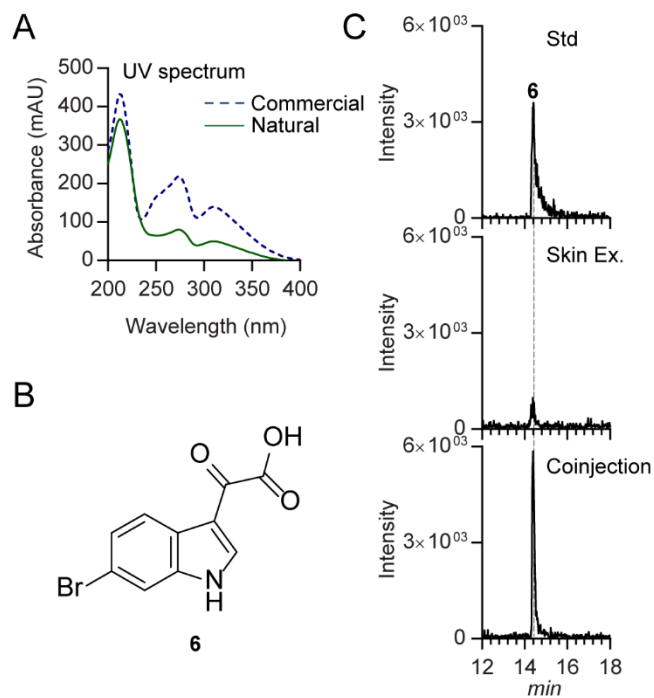
Figure S9. Structural characterization of **6**. (A) UV-visible spectrum of **6**. (B) Chemical structure of **6**. (C) Co-injection with skin extract and standard **6**. Related to Figure 2.
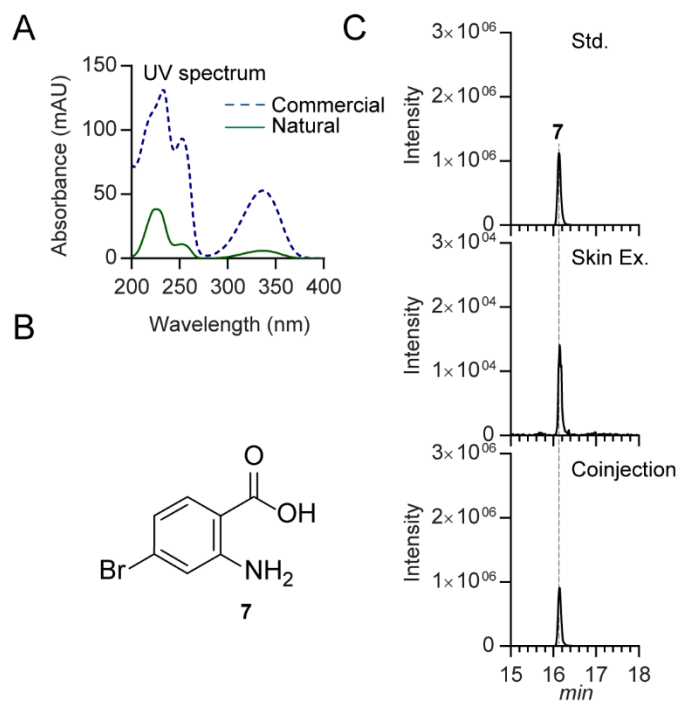
Figure S10. Structural characterization of **7**. (A) UV-visible spectrum of **7**. (B) Chemical structure of **7**. (C) Co-injection with skin extract and standard **7**. Related to Figure 2.
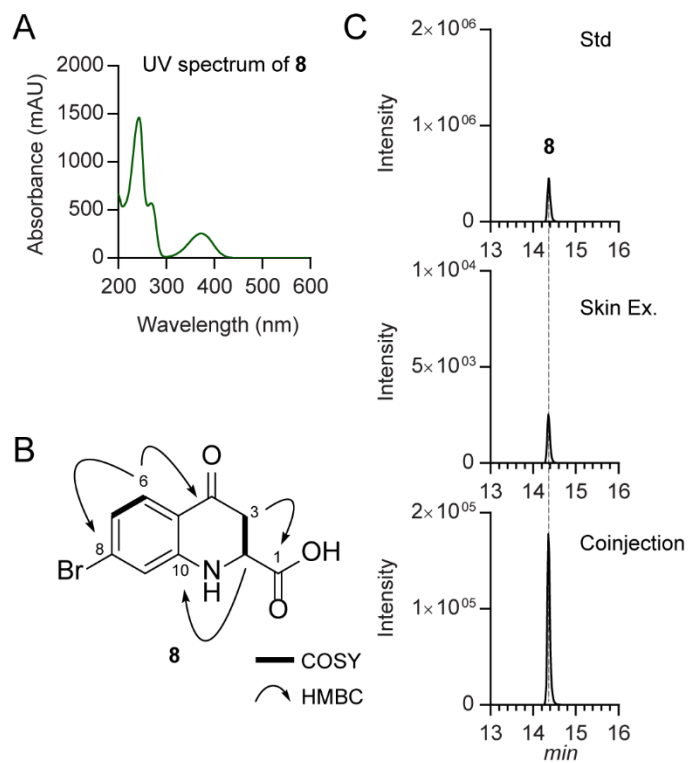
Figure S11. Structural characterization of **8**. (A) UV-visible spectrum of **8**. (B) Key 2D NMR (COSY and HMBC) correlations of **8**. (C) Co-injection with skin extract and standard **8**. Related to Figure 2.
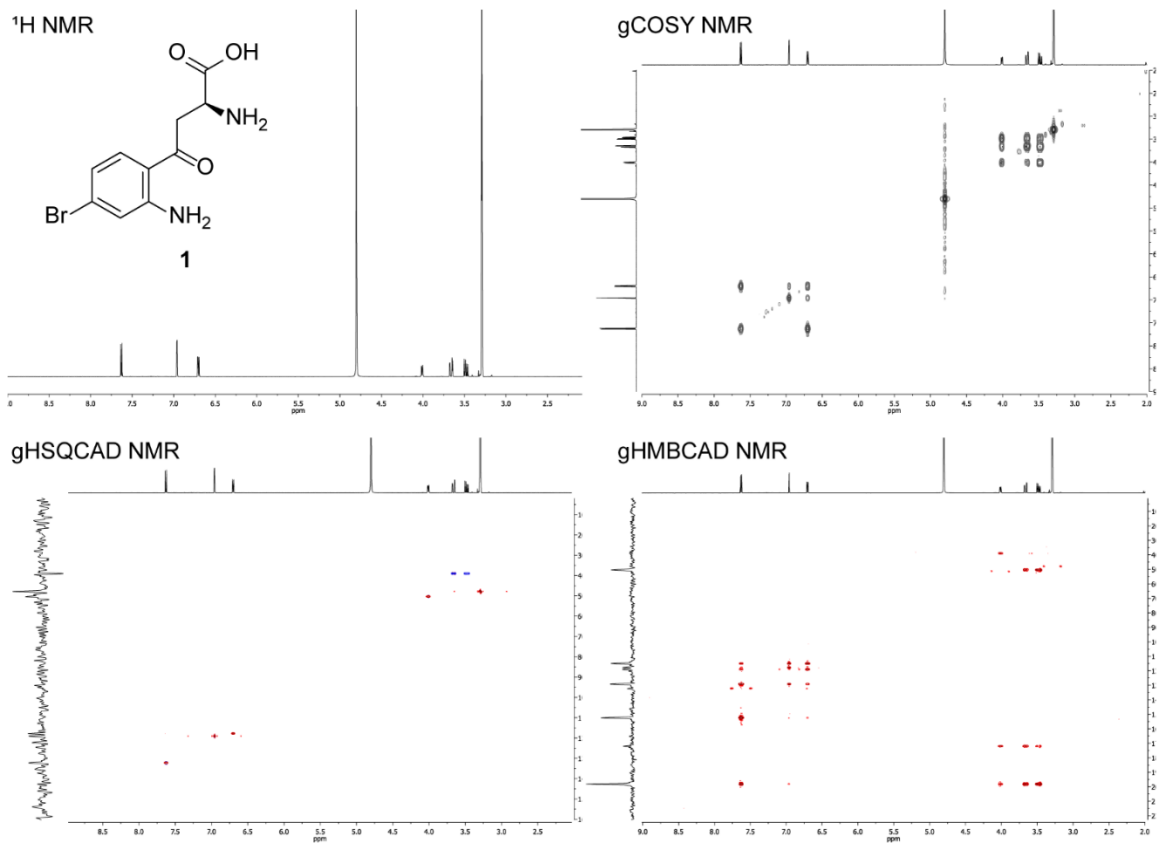
Figure S12. NMR spectra of **1**. Related to Figure 2.
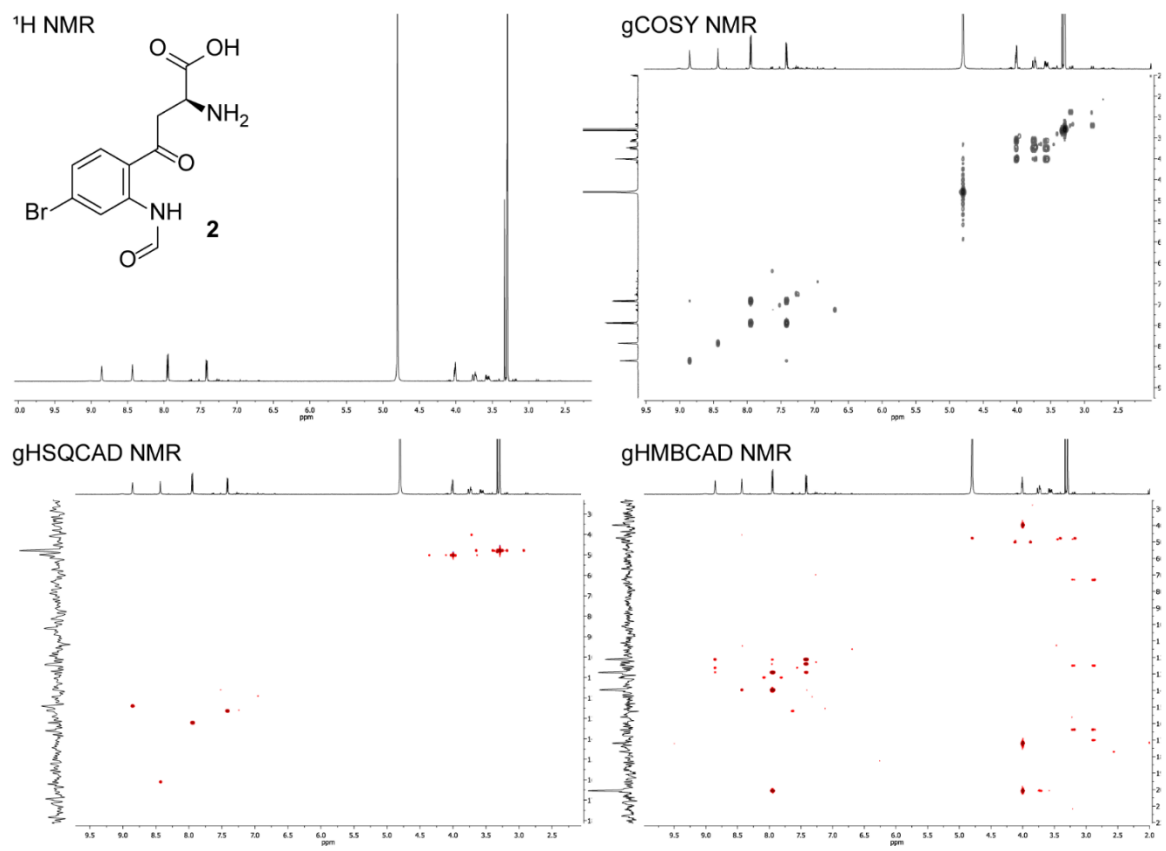
Figure S13. NMR spectra of **2**. Related to Figure 2.
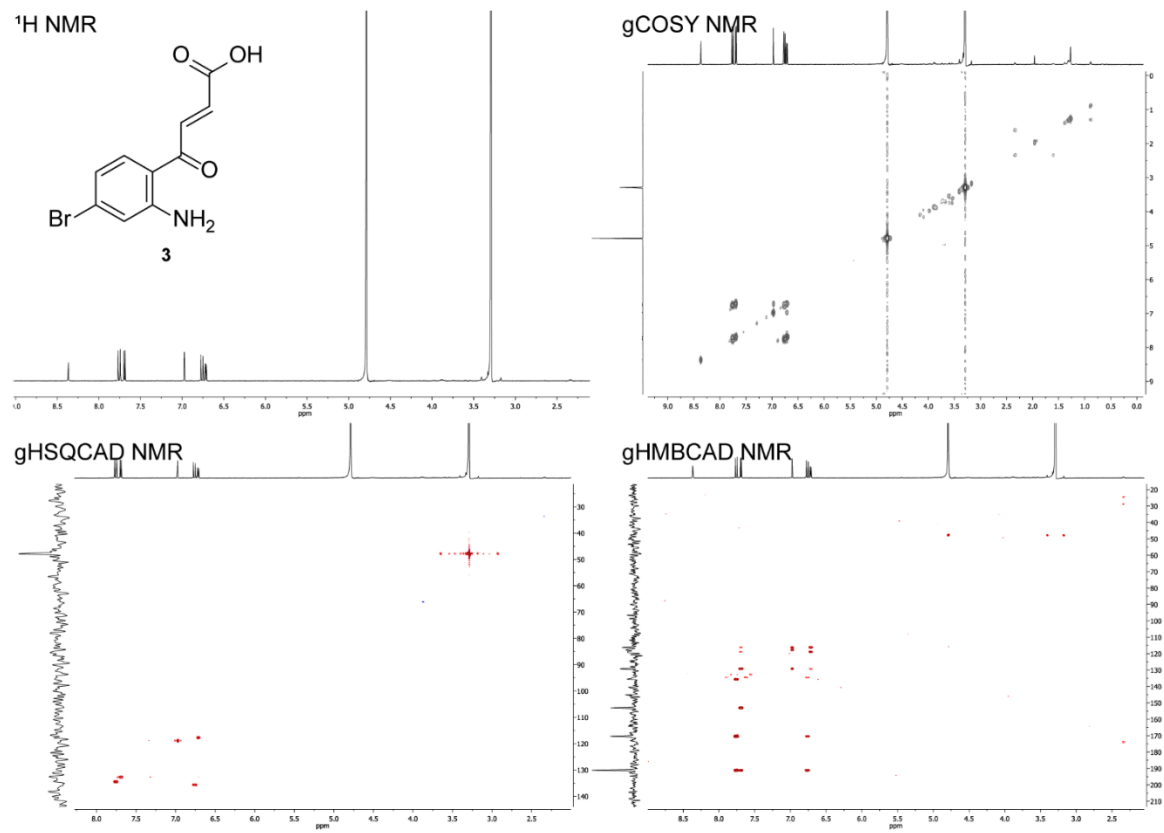
Figure S14. NMR spectra of **3**. Related to Figure 2.
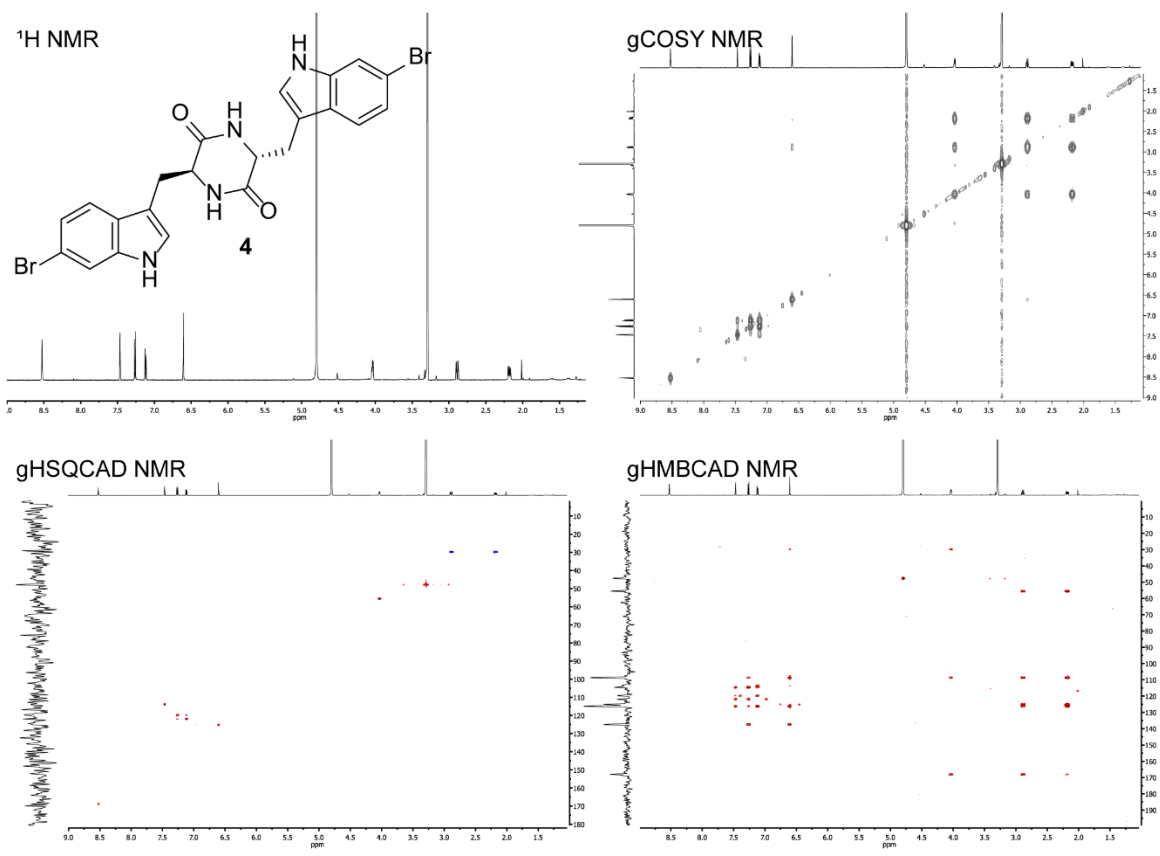
**Figure S15.** NMR spectra of **4**. Related to Figure 2.
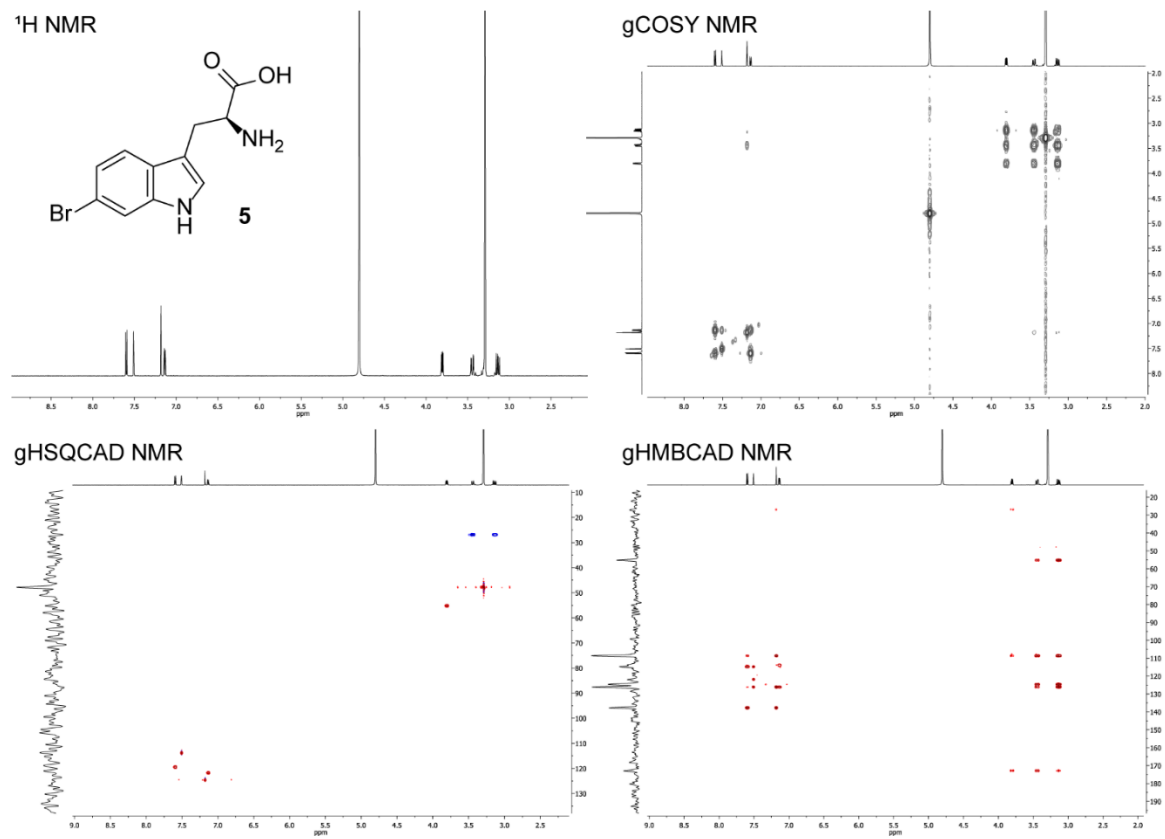
**Figure S16.** NMR spectra of **5**. Related to Figure 2.
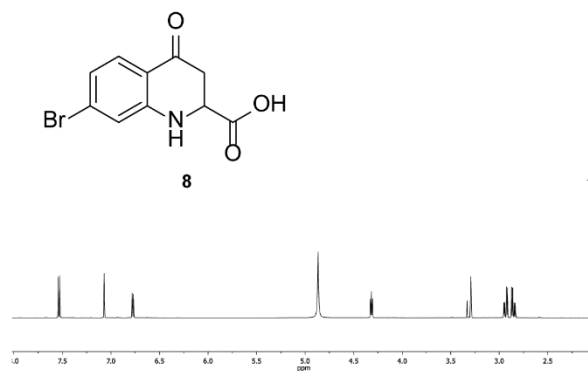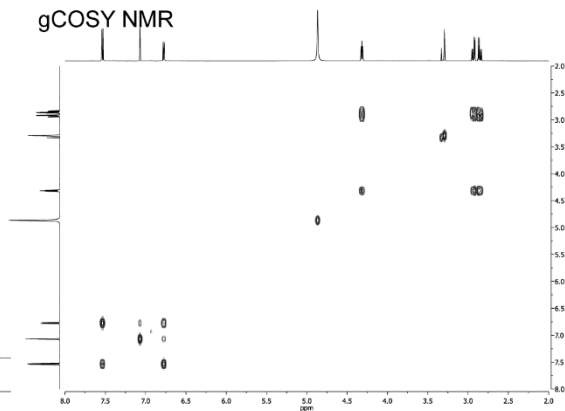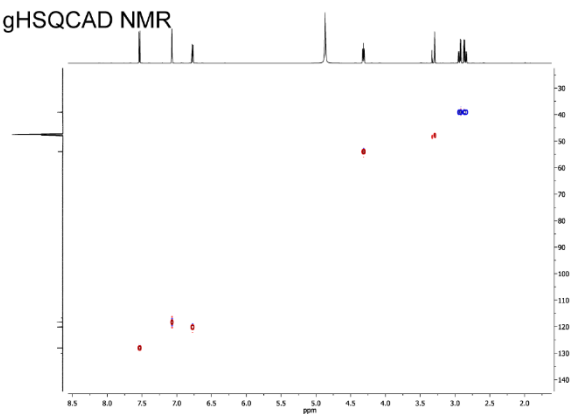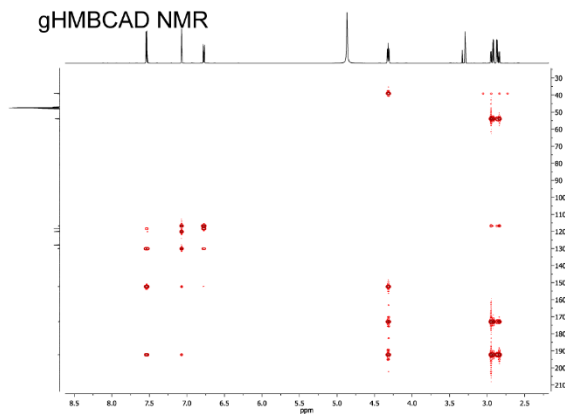
**Figure S17.** NMR spectra of **8**. Related to Figure 2.
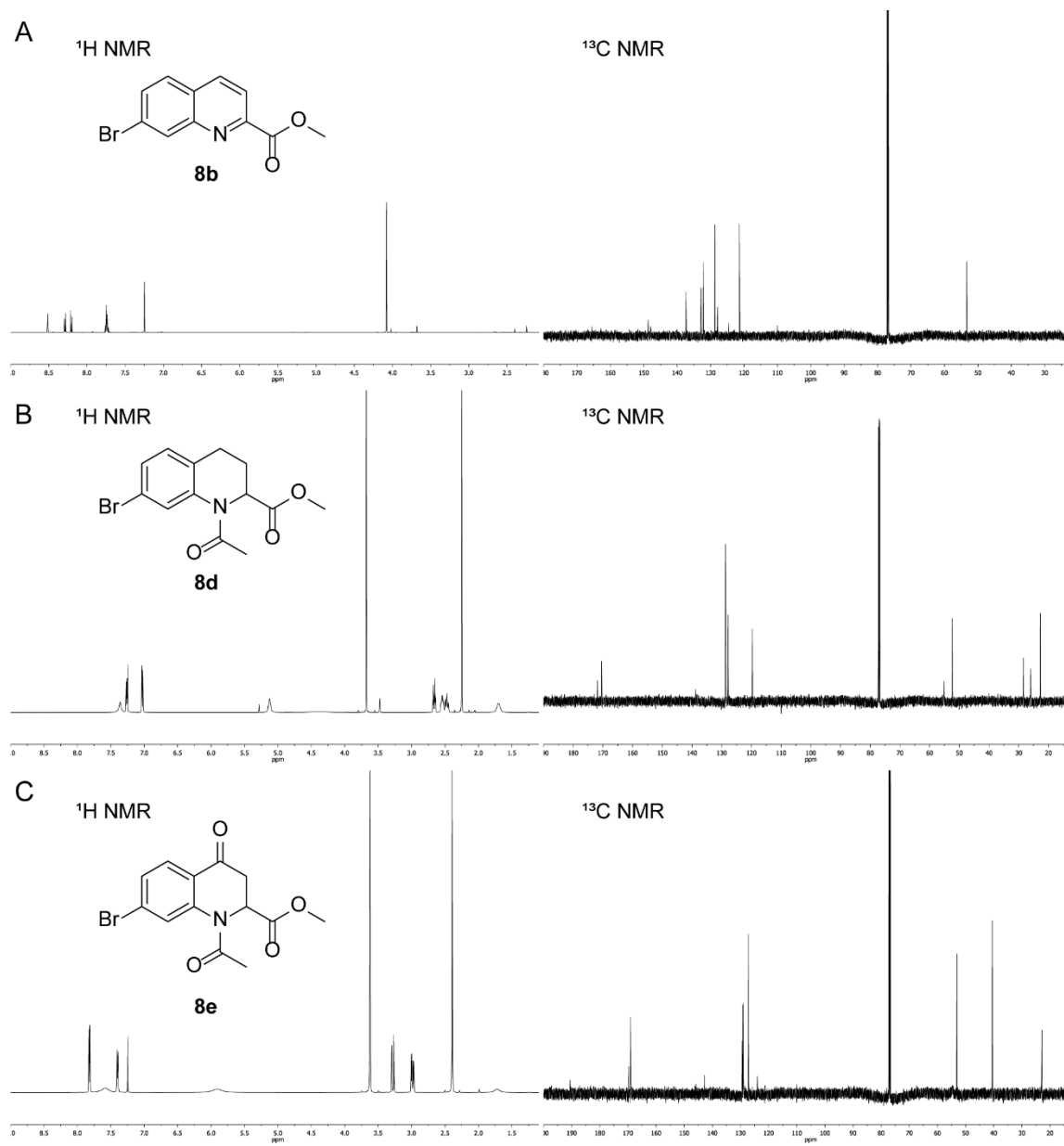
Figure S18. NMR spectra of synthetic intermediates **8b** (A), **8d** (B), and **8e** (C). Related to Figure 2.
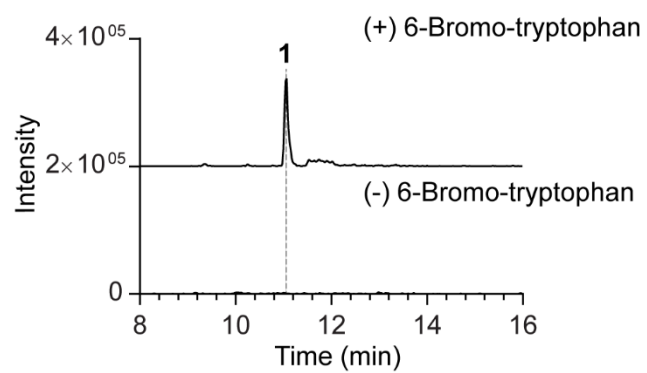
Figure S19. HPLC-MS analysis for the production of 8-bromo-kynurenine (**1**) from *E. coli* culture in the presence and absence of 6-bromo-tryptophan. Related to Figure 4.
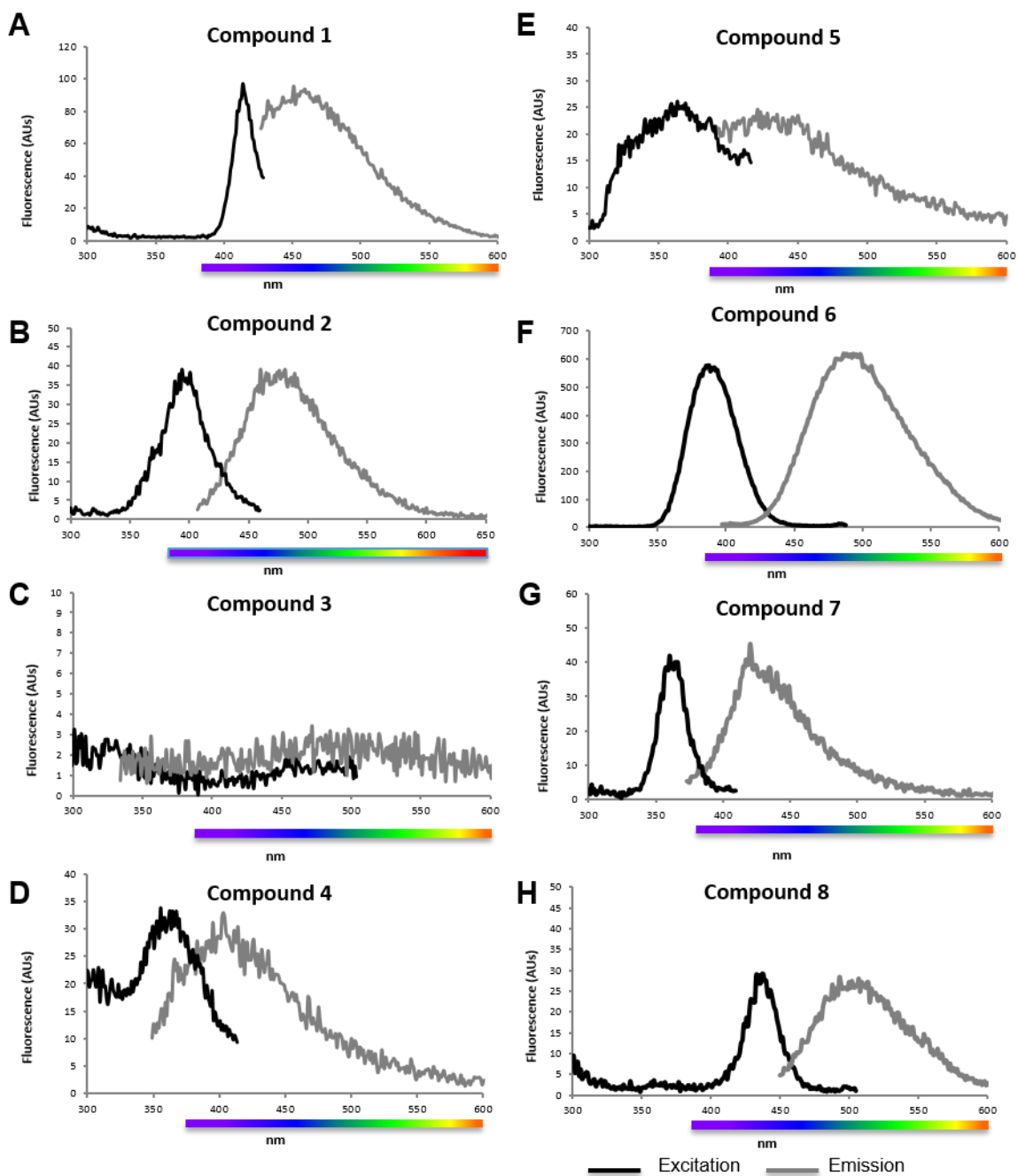
Figure S20. Excitation and emission spectra of compounds **1**-**8** in Phosphate Buffered Saline (PBS). Related to Figure 5.
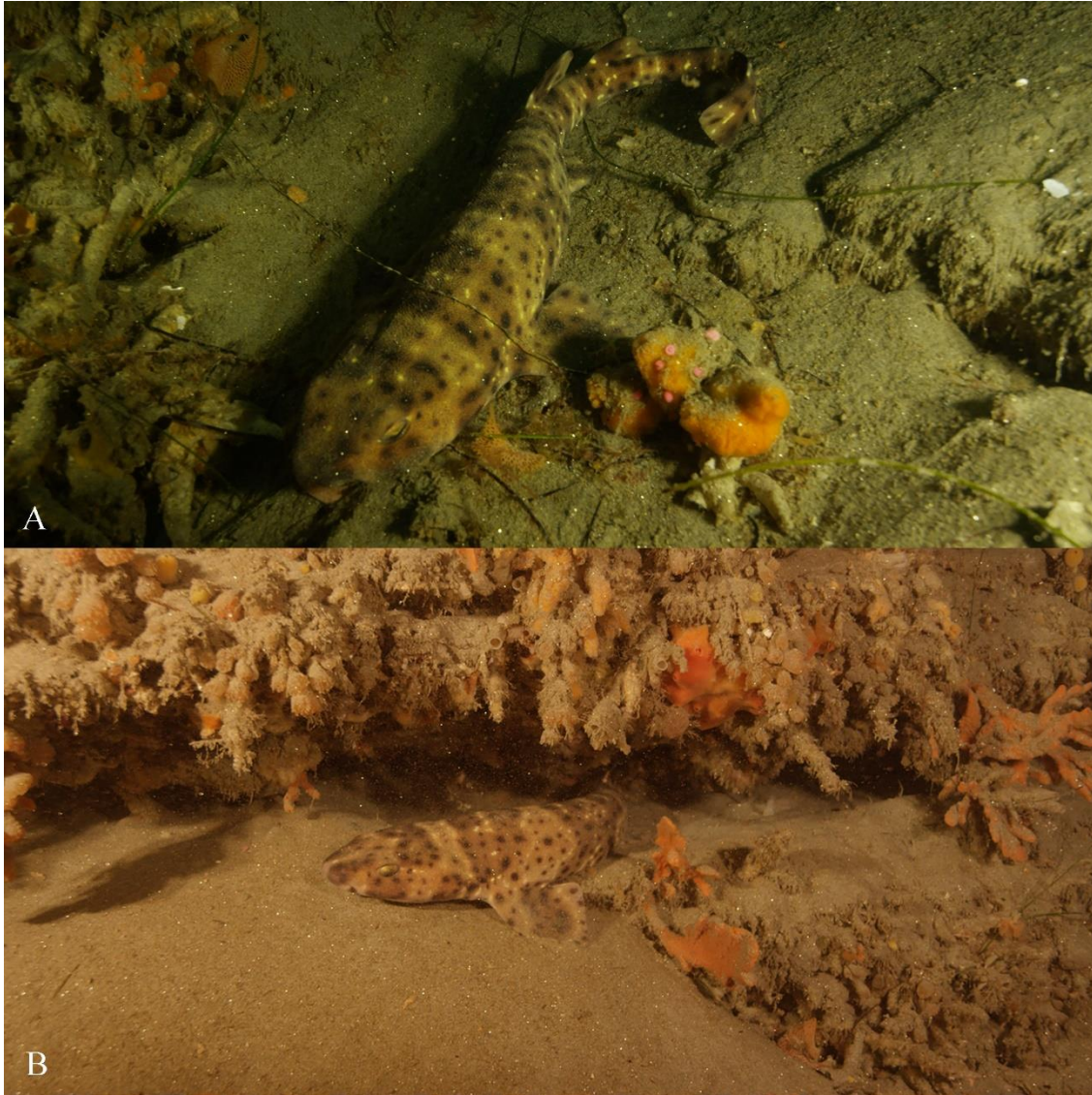
Figure S21. *Cephaloscyllium ventriosum* imagined in their natural habitat in the eastern Pacific, demonstrating their sedentary bottom-dwelling nature. Related to Figure 6.
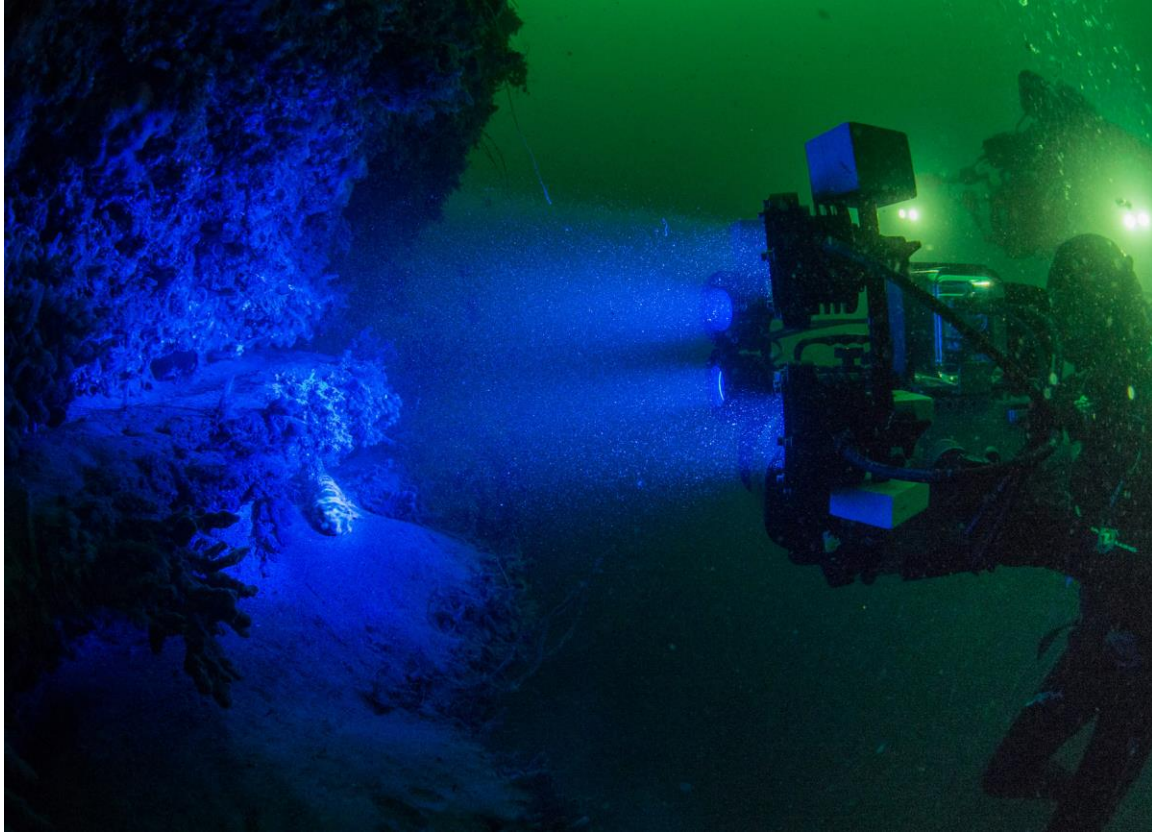
Figure S22. Fluorescent imaging camera system used for *Cephaloscyllium ventriosum* in its natural habitat in the eastern Pacific (30 m, Scripps Canyon, CA). Related to Figure 6.
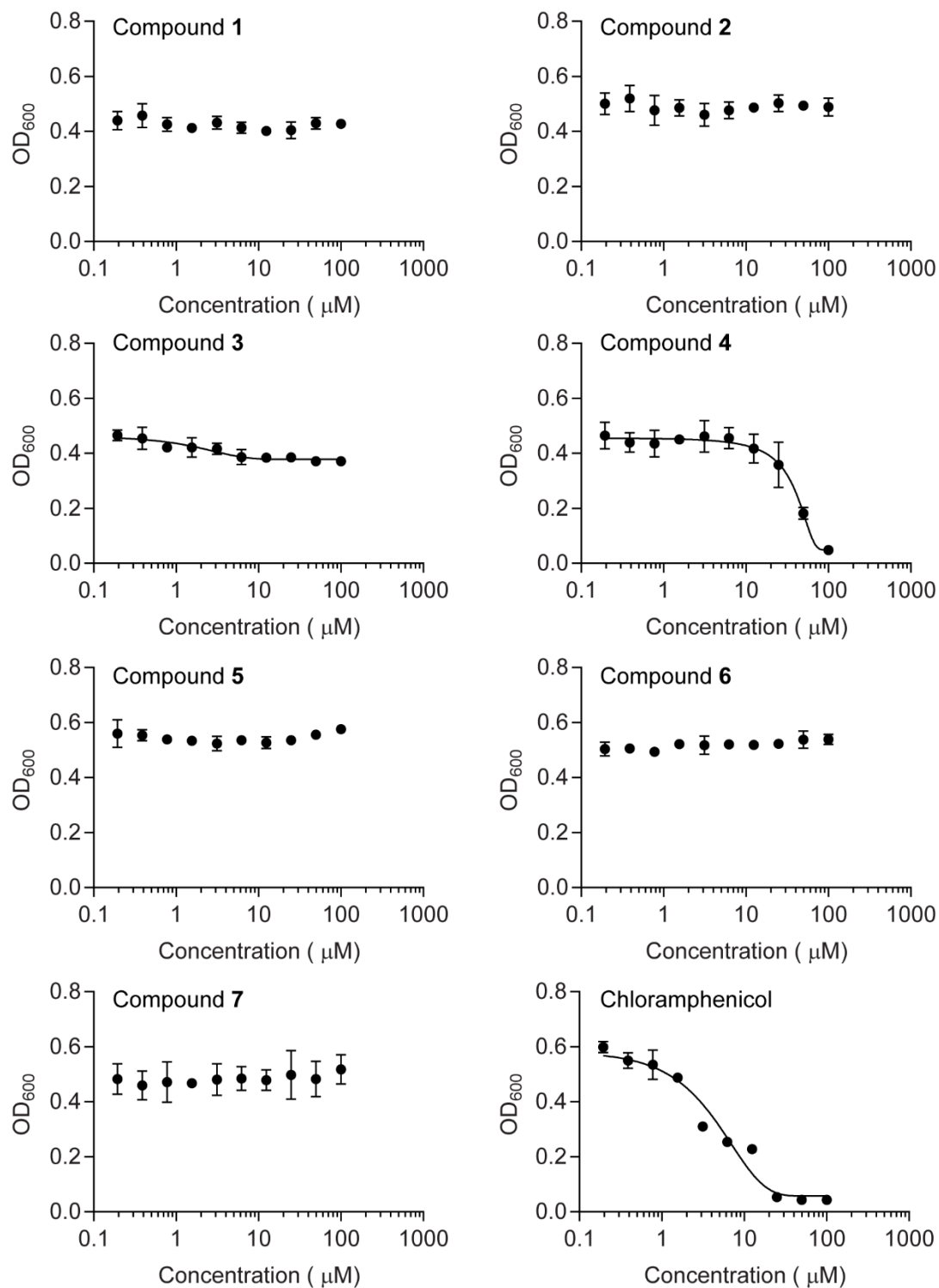
Figure S23. Growth inhibitory assay of metabolites against methicillin-resistant *S. aureus* (MRSA). Related to Figure 6.
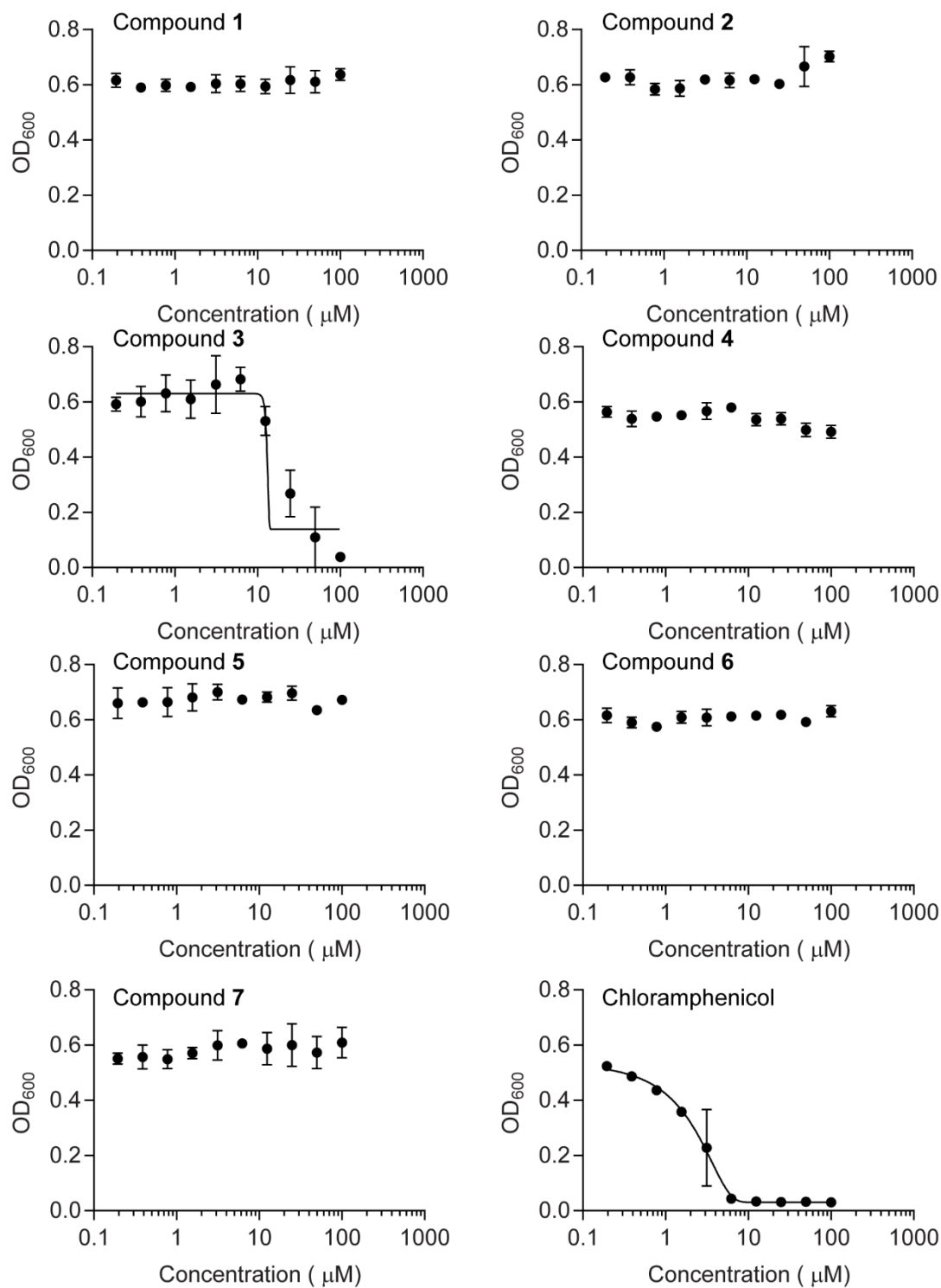
Figure S24. Growth inhibitory assay of metabolites against *Vibrio parahaemolyticus*. Related to Figure 6.
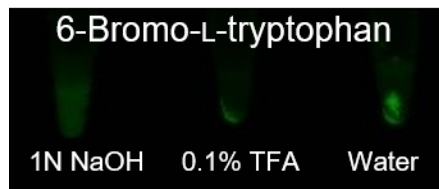
**Figure S25.** Solubility of 6-bromo-L-tryptophan in varying solvents. Figure shows fluorescence image of 6-bromo-L-tryptophan from typhoon instrument with a scanning progress of Alexa Fluor 488. Related to Figure 4.

Table S1. HR-ESI-QTOF-MS data of metabolites **1-8**. Related to Figure 2.

No	Obsd.			Calcd.			Chemical formula
	$[M]^+$	$[M+2]^+$	$[M+4]^+$	$[M]^+$	$[M+2]^+$	$[M+4]^+$	
1	287.0032	289.0013		287.0031	289.0011		$C_{10}H_{11}BrN_2O_3$
2	314.9991	316.9971		314.9980	316.9960		$C_{11}H_{11}BrN_2O_4$
3	269.9777	271.9758		269.9766	271.9745		$C_{10}H_9BrNO_3$
4	528.9875	530.9859	532.9843	528.9875	530.9854	532.9834	$C_{22}H_{18}Br_2N_4O_2$
5	283.0109	285.0090		283.0082	285.0062		$C_{11}H_{11}BrN_2O_2$
6	267.9605	269.9584		267.9609	269.9589		$C_{10}H_6BrNO_3$
7	215.9667	217.9647		215.9660	217.9640		$C_7H_6BrNO_2$
8	269.9748	271.9731		269.9766	271.9745		$C_{10}H_9BrNO_3$

Table S2. NMR assignments of compounds **1**-**3** in MeOD. Related to Figure 2.

No	Compound **1** δ_H mult (J, Hz)	δ_C		Compound **2** δ_H mult (J, Hz)	δ_C		Compound **3** δ_H mult (J, Hz)	δ_C	
1		172.0	C		172.0	C		170.6	C
2	4.01 dd (9.0, 2.9)	50.4	CH	4.01 dd (8.5, 3.3)	50.2	CH	6.76 d (15.4)	135.7	CH
3	3.66 dd (18.5, 2.9) 3.48 dd (18.5, 9.0)	39.0	CH$_2$	3.75 dd (18.6, 3.3) 3.57 dd (18.6, 8.5)	39.9	CH$_2$	7.76 d (15.4)	134.5	CH
4		198.1	C		200.7	C		191.1	C
5		115.0	C		121.2	C		116.2	C
6	7.63 d (8.7)	132.2	CH	7.95 d (8.5)	132.2	CH	7.69 d (8.7)	132.8	CH
7	6.70 dd (8.7, 2.0)	117.8	CH	7.42 dd (8.5, 2.0)	126.4	CH	6.72 dd (8.7, 1.9)	118.0	CH
8		129.2	C		129.2	C		129.2	C
9	6.96 d (2.0)	119.0	CH	8.85 brs	124.0	CH	6.97 d (1.9)	119.0	CH
10		152.5	C		139.8	C		153.1	C
N-formyl				8.43 brs	161.1	CH			

Table S3. NMR assignments of compounds **4** and **5** in MeOD. Related to Figure 2.

	Compound **4**				Compound **5**		
Position	δ_H mult (*J*, Hz)	δ_C		Position	δ_H mult (*J*, Hz)	δ_C	
1, 1'			NH	1			NH
2, 2'	6.60 s	125.1	CH	2	7.18 s	124.6	CH
3, 3'		108.7	C	3		108.7	C
3a, 3a'		126.2	C	3a		126.1	C
4, 4'	7.26 d (8.5)	119.8	CH	4	7.60 d (8.4)	119.5	CH
5, 5'	7.12 dd (8.5, 1.7)	121.9	CH	5	7.14 dd (8.5, 1.7)	121.8	CH
6, 6'		114.6	C	6		114.7	C
7, 7'	7.47 d (1.7)	113.8	CH	7	7.51 d (1.6)	113.9	CH
7a, 7a'		137.4	C	7a		137.8	C
8, 8'	2.89 dd (14.5, 3.8)	29.8	CH_2	8	3.44 dd (15.3, 4.2)	27.0	CH_2
	2.18 dd (14.5, 7.1)				3.14 dd (15.3, 9.0)		
9, 9'	4.04 dd (7.0, 3.9)	55.6	CH	9	3.81 dd (9.0, 4.2)	55.3	CH
10, 10'		168.1	C	10		172.8	C

Table S4. NMR assignments of compound **8** in MeOD. Related to Figure 2.

No	δ_H mult (J, Hz)	δ_C	
	Compound **8**		
1		173.0	C
2	4.32 m	54.0	CH
3	2.93 dd (16.5, 6.0)	39.1	CH_2
	2.85 dd (16.5, 7.5)		
4		192.3	C
5		116.8	C
6	7.54 d (8.5)	128.0	CH
7	6.78 dd (8.5, 1.5)	120.2	CH
8		130.1	C
9	7.07 d (1.5)	118.4	CH
10		152.4	C

Video S1. Footage of *Cephaloscyllium ventriosum*. Related to Figure 1.

Reference

Gruber, D.F., Loew, E.R., Deheyn, D.D., Akkaynak, D., Gaffney, J.P., Smith, W.L., Davis, M.P., Stern, J.H., Pieribone, V.A., and Sparks, J.S. (2016). Biofluorescence in catsharks (Scyliorhinidae): Fundamental description and relevance for elasmobranch visual ecology. Sci. Rep. 6, 24751.